"STUDY OF CONCEPTUAL AND OPERATIONAL FEASIBILITY OF LASER DOPPLER DETECTION SYSTEMS"

Progress Report

To November 30, 1970

Contract No. NAS 8 - 24810
DCN 1-9-75-10090 (1F)

RESEARCH INSTITUTE FOR ENGINEERING SCIENCES

COLLEGE OF ENGINEERING

WAYNE STATE UNIVERSITY

DETROIT, MICHIGAN

48202

RIES

"STUDY OF CONCEPTUAL AND OPERATIONAL FEASIBILITY OF LASER DOPPLER DETECTION SYSTEMS"

Progress Report

To November 30, 1970

Contract No. NAS 8 - 24810
DCN 1-9-75-10090 (1F)

Principal Investigator: J. Alex Thomson

RESEARCH INSTITUTE FOR ENGINEERING SCIENCES
College of Engineering
Wayne State University
Detroit Michigan 48202

INTRODUCTION

This report covers effort on Contract No. NAS 8 - 24810 up to November 30th, 1970. It is divided into three parts, 1) a brief summary of completed efforts, 2) a summary of efforts currently in progress, and 3) a summary of various activities: meetings, reviews etc. It also contains a separate Appendix, RIES Report No. 70-1.

This report was prepared by Wayne State University under Contract No. NAS 8 - 24810 - "Study of Conceptual and Operational Feasibility of Laser Doppler Detection Systems," for the George C. Marshall Space Flight Center of the National Aeronautics and Space Flight Administration. The work was administered under the technical direction of the Aero-Astrodynamics Laboratory, George C. Marshall Space Flight Center.

CONTENTS

1. SUMMARY OF COMPLETED PROJECTS

In this section abstracts of a number of completed projects are listed. Reports on these projects are included in detail as Section 4 of this report.

i) Amplitude modulation and transient time effects

The frequency spreading effects of amplitude modulation due to convenction of aerosols through the coherence volume are discussed. It is shown that the frequency spread due to amplitude modulation is independent of particle density for randomly distributed particles. The spread increases as the coherence volume decreases. For a focused system the frequency spreading for an f/1 system (focal volume dimension of order of a wavelength) is comparable to the Doppler shift and effectively prevents accurate measurement of velocity. This effect limits the spatial resolution that can be achieved by a laser Doppler measurement instrument and is important in thin boundary layers. Limiting spatial resolutions are calculated for various applications and geometries.

For a non-scanning or slowly scanning system, this amplitude modulation provides a mechanism for determining the velocity component perpendicular to the line of sight. Here since the frequency broadening of the signal is directly related to the transit time through the coherence volume, a precise knowledge of the dimensions of this volume allows determination of the perpendicular velocity. Thus such a system has the capability of obtaining both the velocity component parallel to the line of sight (w) and the speed perpendicular to the line of sight (u). Since the mean value of the fluctuating component of the product of these two velocities $\left\{(u - \bar{u})(w - \bar{w})\right\}$ is directly proportional to the turbulent stress parallel to the line of sight a data processing method for evaluating this quantity allows a direct measure of this stress. This would be of particular value for atmospheric boundary layer measurements.

ii) Diagnostics of the backscatter signal for a long range pulsed system.

For a pulsed system, the turbulence level at given range points is manifested through two effects: 1) the spectral broadening of the signal returning from a given range element, and 2) the fluctuation in the mean velocity or mean frequency from range element to range element. The finite pulse length imposes an inherent spectral spread in the returning signal. Since the power spectrum of the turbulent velocities generally increases at increasing spatial scale, the fluctuation from range point to range point of the mean velocity will generally be greater than the frequency spread of the signal returning from any given range element. Thus for low levels of turbulence where the Doppler spreading of the signal is small it will be more appropriate to determine the turbulence level from the variation of the mean velocity as a function of range rather than the spread of the signal coming from any given range element. This implies that an adequate diagnostic system would be one which simply measured the mean frequency of the returning signal, as a function of range.

iii) Feasibility study of detection of stratospheric motion by a ground based 10.6μ laser Doppler detection system.

The potential for measurement of stratospheric motion and turbulence using a ground based 10.6μ pulsed laser Doppler system is discussed. Expected signal-to-noise ratios are estimated and comparisons are made with high-power radar detection systems. Although the signal-to-noise ratios for the CO_2 laser and the radar systems are dependent on different parameters, the two systems appear to have comparable capability under good optical seeing conditions (i.e. night time).

iv) Two phase flow effects.

Rough estimates are given for the conditions under which the aerosol particles mimic the fluid motion and it is shown that there usually exists a broad range of particle radii for which the particles follow the fluid. Very large particles fail to follow the fluid motion at high frequencies because of their inertia, and very small particles exhibit an added velocity due to Brownian motion.

v) General considerations concerning laser Doppler systems for aircraft wake detection.

The estimated characteristics of a particular laser Doppler system for scanning operation are presented. Range resolution characteristics, signal-to-noise, and data rate are estimated. For the system considered a mean signal-to-noise of 150 per meter length in the coherence volume is estimated, although this parameter is highly sensitive to some of the properties assumed.

vi) Acoustic scattering from turbulent aircraft wakes.

The potential of an atmospheric sonar system for detection of aircraft wakes is evaluated. A turbulent vortex wake is assumed and the cross section per unit volume estimated parametrically. Both forward scatter bistatic systems and backscatter systems are considered. The signal power is compared to typical background noise powers and estimates for the signal-to-noise (i.e. signal-to-background) are given.

vii) Aircraft wake fluid dynamics.

An analysis is in progress to develop a theory for the structure and decay of turbulent line vortices. A portion of this analysis is an extension of the theory of Hoffman and Joubert to allow treatment of the core region and to account for the axial decay of the vortex. The initial approach is to assume a completely turbulent vortex, introduce a Prandtl

mixing length hypothesis, consider turbulent transport only in the radial direction but allow convection both radially and axially (and of course tangentially). Of primary interest is the axial decay of the vortex and the phenomena of vortex breakdown. The analysis has been formulated and effort is currently in progress to obtain both approximate and "exact" solutions. The equations for similarity solutions have been formulated for the full set of equations. The present analysis is proceeding in two directions: 1) to solve for the self similar solutions, and 2) to divide the vortex structure into three regions: an inner core, an intermediate self-preserving region, and an outer region. In the intermediate region the turbulent stresses are high, and radial and axial convection of momentum can be neglected. This assumption leads to the self-preserving logarithmic growth of the circulation with radius predicted theoretically and confirmed experimentally by Hoffman and Joubert. In the inner region the axial velocities can be shown to be comparable to the tangential velocities and convection of momentum cannot be ignored. That the axial and tangential velocities are indeed of comparable magnitude in aircraft wake vortices is apparently evident in some of the smoke visualization pictures taken recently at NASA-MSFC by NASA. In order to compare with the theoretical development it would be highly desirable to obtain quantitative reduction of these photographs in terms of rotation velocities and axial velocities as a function of radius and distance downstream of the aircraft. If further flights should be scheduled, it is suggested that photographic coverage be obtained with a clock and with distance scales in the field of view. Also the ambient wind velocity should be measured, and the aircraft lift and drag needs to be known.

It would also be desirable to obtain motion picture coverage from two different stations so that stereo reduction is possible. This is of particular importance at vortex breakdown where there has been some indication of negative rotations.

viii) Wake modelling and simulation.

Requirements for experimental simulation of aircraft wakes in a laboratory environment are examined. Three particular systems were considered - a wind tunnel, a water tunnel, and a water tow basin. The simulation facilities were required to satisfy various constraints including sufficiently high Reynolds numbers that the effects of molecular viscosity were negligible, a test time long compared with any expected instability of decay time, swirl values (ratio of axial to peak tangential velocity) covering the flight range. The major disadvantage of the tow basin is that the flow is unsteady and the time available for measurements is limited. Thus for detailed probing of the wake a tunnel is probably preferred. However, for preliminary measurements aimed at establishing the validity of the simulation, the tow basin appears to be an effective approach.

2. CURRENT EFFORTS

i) Laser Van Optics

The optical mechanical system for the laser van is being designed. The design goal is to provide capability for operation in both a focused coaxial mode and a focused or partially focused bistatic mode. The major design problem in the bistatic system is concerned with the beam steering, mirror sensing and steering mechanisms, which must be accurate enough to control the pointing error in at least one plane to be less than the diffraction limit. At present it appears that for a confident design it will be necessary to carry out preliminary experiments to define these steering and sensing mechanisms. The present design envisages 6" diameter telescope optics for the initial prototype design, but the system is to be constructed to allow an increase to 12" optics with minimal additional construction.

A detailed description of the optical/mechanical considerations is being prepared and will be issued shortly.

ii) Systems Modelling

Calculations are currently being carried out to obtain detailed profiles for the system radial and axial response for various operating conditions and methods, and aperture apodization functions. These calculations are being incorporated into a computer program. When this modelling is completed the calculations will be extended to pulsed systems and will be developed in the form of a computer program that will permit arbitrary specifications of the aerosol density distribution. The output of the program will essentially be the voltage at the output of various finite width frequency filters.

iii) Laser Van Experimental Program Plan

A set of specific experiments and experimental objectives for the laser van system has been compiled. This includes preliminary experiments to define the optical characteristics, the effect of finite particle density, effects of finite scattering rates, the effects of turbulence, and the effects of signal-to-noise. A preliminary set of some of these measurements was recently carried out at NASA-MSFC. A more extensive set of experiments will be suggested for implementation at Colorado State University. Some consideration has been given to the non-scanning vertical or near-vertical beam system for obtaining measurement of real or simulated aircraft vortices. The present van system at Colorado State or the one currently under construction would both be adequate for this measurement.

iv) Standard Scattering Source

A source that can be used as a standard scatterer is being constructed. The intent is to provide a source that is calibrated both in scattering amplitude and velocity. The system is essentially a small wind tunnel with open ports on either side of the test section for entrance of the laser beam. An aerosol source is located on the centerline at the mouth of the wind tunnel, and ejects a controlled fine stream of aerosols along the wind tunnel axis. The wind tunnel itself is almost completed.

3. SUMMARY OF MEETINGS, REVIEWS, ETC.

1969

May 24-27	Technical discussions and outline of contractual effort, at NASA-MSFC, Dr. J.A.L. Thomson.
June 4 - 6	Technical discussions regarding the laser Doppler system, at NASA-MSFC, Dr. J.A.L. Thomson.
Aug. 5 - 8	CAT reviews at NASA-MSFC, Dr. J.A.L. Thomson, Dr. A.J. Glass, Dr. A. Scaglione.
Oct. 16	CAT system review at Raytheon, Mass., Dr. J.A.L. Thomson and Dr. A.J. Glass.
Nov. 5	CAT system review at NASA-MSFC, Dr. J.A.L. Thomson.

1970

Mar. 16-18	Technical discussions at NASA-MSFC, Dr. J.A.L. Thomson.
May 12-16	Further technical discussions at NASA-MSFC, Dr. J.A.L. Thomson.
Sep. 1-4	Aircraft Wake Turbulence Conference at Boeing, Seattle, Dr. J.A.L. Thomson.
Sep. 23-27	CAT and aircraft wake review at NASA-MSFC, Dr. J.A.L. Thomson.
Oct. 3 - 6	Technical discussions at University of Florida and NASA-MSFC - Dr. J.A.L. Thomson.
Nov. 7 - 9	Technical discussions concerning the laser van measurements and optical design, at NASA-MSFC, Dr. J.A.L. Thomson and Dr. A. Deepak.
Nov. 12-13	CAT system review at Raytheon, Mass., Dr. J.A.L. Thomson.

"STUDY OF CONCEPTUAL AND OPERATIONAL FEASIBILITY OF LASER DOPPLER DETECTION SYSTEMS"

Appendix

to

Interim Progress Report

To November 30, 1970

Contract No. NAS 8 - 24810

DCN 1-9-75-10090 (1F)

by

J. Alex Thomson

RESEARCH INSTITUTE FOR ENGINEERING SCIENCES

College of Engineering

Wayne State University

Detroit, Michigan 48202

"Study of Conceptual and Operational Feasibility of Laser Doppler Detection Systems"

This report was prepared by Wayne State University under Contract No. NAS 8 - 24810 - "Study of Conceptual and Operational Feasibility of Laser Doppler Detection Systems," for the George C. Marshall Space Flight Center of the National Aeronautics and Space Administration. The work was administered under the technical direction of the Aero-Astronautic Laboratory, George C. Marshall Space Flight Center.

TABLE OF CONTENTS

I. BACKGROUND

The purpose of the present study is to carry out a comprehensive review and analysis aimed at establishing the feasibility and design criteria of a laser doppler system for detecting and mapping turbulence levels and wind or velocity profiles in various applications. Of particular interest are systems for detecting clear air turbulence at high altitudes and systems for mapping local atmospheric velocity distributions (ground winds) in the neighborhood of large jet airports, VTOL and helicopter landing areas. In addition to the laser doppler technique other remote sensing systems have been evaluated.

Clear Air Turbulence

Clear air turbulence at high altitudes presents a potential hazard to aircraft and passengers. It is presently believed that such turbulence can occur in regions of relatively high wind shear when the destabilizing effect of the shear is sufficient to overcome the natural stability of a positive potential temperature gradient. Strong turbulence appears to be associated with regions of moderately high thermal stability which requires a high local wind shear to result in a transition to turbulence. The kinetic energy available to be released into turbulent motion under these conditions can be considerably greater than when only a weak shear is required to induce

instability. True turbulence is not the only hazard to high altitude aircraft. Regions of strong laminar shear may themselves create a hazardous environment.

Many techniques have been and are being evaluated as possible methods for detecting turbulence at sufficient range that evasive action or rerouting of the flight can be accomplished. These include, in part, high powered radar (ground based and airborne, monostatic and bistatic), passive infrared detection, scintillation of exoatmospheric sources, incoherent and coherent lidars. At these high altitudes a radar signal is scattered by inhomogeneities of the atmospheric refractive index (which, at tropopause altitudes, are due to temperature fluctuations). The laser techniques depend on natural aerosols to provide scattering centers. Spatial variations in the thermal emissions from the atmosphere can indicate regions of strong temperature gradients which may be associated with regions of turbulence. Passive radiometric detection of such gradients has been accomplished in flight, although a one-to-one correspondence between the existence of temperature gradients and turbulence has not yet been established.

The disadvantage of passive IR techniques is that they yield only limited range information and respond only to relatively broad thermal inhomogeneities. Inhomogeneities seen on radar are of the order of the radar wavelength in size and are more likely to be associated with turbulence. Doppler radar and doppler lidars respond directly to the convective motion and can give direct information about the velocity spectrum (although in the case of radar the time dependent growth and decay of the eddies renders the connection only approximate).

The scattering crossection per unit volume is sufficiently small at high altitude that high powers are needed for active radar and lidar systems. For a radar system the backscatter cross section per unit volume from a region of Kolmogoroff turbulence is

$$d\sigma/dV \simeq 0.06\, C_n^2\, \lambda^{-1/3} \text{ cm}^2/\text{cm}^3\text{-ster} \qquad (1.1)$$

Taking a value of $C_n^2 = 3.5 \times 10^{-16}$ cm$^{-2/3}$ as a typical tropopause value, we find the backscatter cross section for 6 cm radar to be about 1.1×10^{-17} cm^2/cm^{3}ster.

For comparison it is interesting to estimate the comparable quantity for lidar backscatter from aerosols. The aerosol backscatter cross section per unit volume is $n\sigma$ where n is the aerosol concentration and σ the backscatter cross section. The value of $n\sigma$ is not well known at 10.6μ at the tropopause. For a rough estimate we assume a density of $10^3/m^3$ and a cross section per particle of 3×10^{-8} cm^2. For these values the 10.6μ aerosol backscatter cross section per unit volume is about 2.5×10^{-12} cm^2/cm^3-ster, i.e., about 2×10^5 times larger than the radar cross section from the same region. Thus it is apparent that light scattering is an effective detection method compared to airborne radar (assuming comparable output power capabilities). However, for ground based systems, radars which can utilize high powers and large apertures may provide superior detection capability.

Other methods for detecting turbulence at high altitudes have been suggested, such as scintillations of extra terrestrial sources, fluctuations in absorption along the line of sight. However, the difficulty of arranging for suitable sources of radiation and the problem of avoiding long measurement times and high precision measurements to extract range

information (by inversion or crossed beam techniques, for example) render these methods somewhat unsatisfactory, at least for high altitude CAT.

Low Altitude Winds due to Aircraft Wakes

In comparison with the problem of detecting high altitude CAT at long ranges, the problem of detecting and measuring ground winds at moderate ranges is expected to be relatively simple as far as signal to noise is concerned. The major problems are in the area of finding methods for obtaining good spatial and velocity resolutions, in the methods for scanning the volume of interest, and the methods for data handling and data presentation.

In the present study we have examined methods for detecting and mapping such wind structures in the vicinity of large jet airports. In addition to the laser doppler method, we have examined the potential of acoustic monostatic and bistatic techniques and intend to evaluate cross beam correlation, passive IR radiometry techniques. Application is intended to trailing vortices as well as to wind gust problems experienced by VTOLs and helicopters.

Heterodyne Doppler Detection of Clear Air Turbulence

The analysis of a system designed for the detection of clear air turbulence using heterodyne detection of a scattered laser signal proceeds along identical lines to the analysis of a laser radar system. The properties of the return signal must first be identified. Knowing the intensity and frequency distribution of the return signal, and the propagation characteristics of the intervening atmosphere, one can calculate the signal strength at the receiving optics in terms of the radiated power. The detection system must then be analyzed to determine the effective signal-to-noise ratio, and to

ascertain the radiated power required to obtain a specified set of performance characteristics. A determination must also be made of the optimal mode of operation: CW, pulsed CW or Q-switched. The advantages of multiple modes of operation must be weighed against the added cost and complexity of a more flexible system.

A preliminary analysis of several of the factors involved in the scattering and detection process has previously been carried out.[1] That analysis demonstrated that, in order to detect high altitude atmospheric turbulence at long range with a laser doppler system, careful attention to the instrumental design is mandatory. Successful performance in an operational system will probably require achievement of performance moderately close to theoretical in the design. Orders of magnitude loss in achievable signal to noise can result from imperfect or erroneous choice of optical design. At low to moderate altitudes, long wavelength operation is strongly to be preferred principally because of the relatively greater degradation of the propagating signal by both atmospheric turbulence and extinction by scattering at short wavelengths.

In addition, since the power signal to noise is proportional to the number of photons detected, a 10.6μ CO_2 laser inherently has a considerable advantage over a visible laser at the same power. These facts, coupled with the present availability of high power infrared lasers and the low sensitivity of long wavelength interferometers to vibration and misalignment, press strongly for long wavelength operation.

CW Doppler heterodyne detection at 10.6μ has been demonstrated by several groups[2,3] and operating optical radar[4] and

communications[3] systems have been constructed. By careful detector design, bandwidths as high as several gigahertz have been achieved[3] using copper-doped germanium at 4.2 K, and in excess of 10 MHZ with gold-doped germanium at 77 K. Estimates made in Ref. 1 indicate that the bandwidth required for detection from a stationary platform is 4 MHZ, while from a platform moving at 300 m/sec, an additional frequency offset of 60 MHZ would be required. It is interesting to compare this requirement with the characteristics of the communications system reported in Ref. 3. The modulation bandwidth of that system was 5 MHZ, and the local oscillator was offset 30 MHZ from the transmitted signal. (This system is an FM television system.) The laser employed was a sealed-off CO_2 laser radiating 6 to 8 watts in a single mode, with a frequency stability of ± 1 MHZ over a period of several hours. The only significant drawback to the use of this system for the purposes envisioned in this study is the fact that the detector is Cu:Ge at 4.2 K.

There is some possibility of producing higher powers from mode-controlled, sealed-off CO_2 laser systems. Witteman[5] has reported 60 watts from a tube 152 cm long, sealed-off, but equipped with a water replenisher. Clearly, an area to pursue in further investigation is the development of stable, high power, sealed-off laser oscillators and amplifiers.

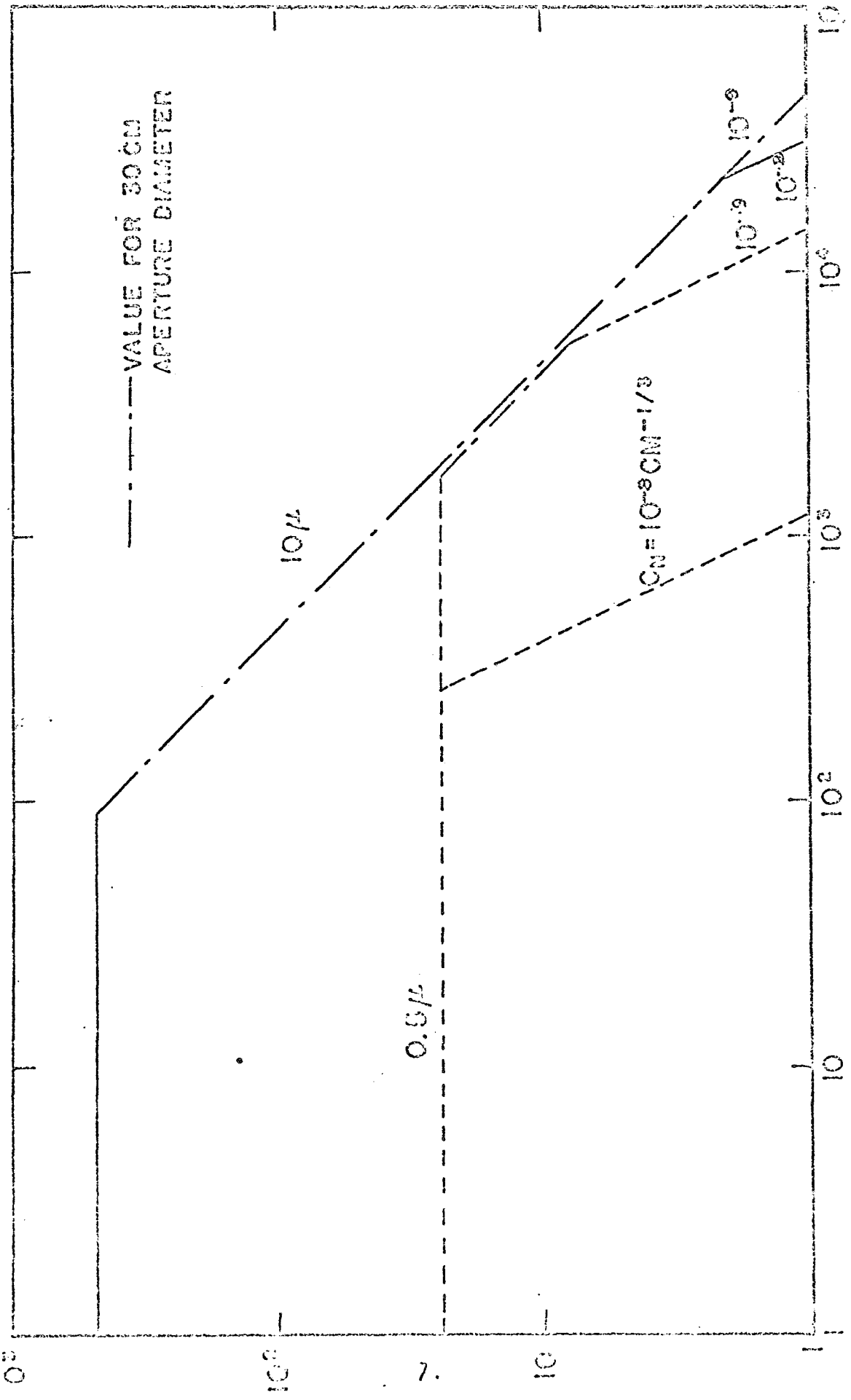

Figure 1.1 Signal-to-Noise per Joule vs Range and Turbulence Level for Horizontal Path at 10 km Altitude.

A few comments on the results of conclusions reached in Ref. 1 are in order. In Fig. 1 (reproduced from Ref. 1) we show the calculated S/N expected for detection of atmospheric aerosols at 10 km altitude as a function of range. (Since the value of $\overline{n\sigma}$ at 10.6 microns and at this altitude is not well known, the value of S/N is subject to some uncertainty). The estimates leading to these values for S/N are felt to be fairly conservative as far as the instrument is concerned (i.e. pessimistic).

These values of S/N were calculated for a coaxial system in which the transmitter and receiver use the same external optics. Such a system is quite desirable for pulsed, modulated or focused systems which have a rapid search rate or scan requirement. However, it is difficult to avoid two 50% losses at the combining beam splitter with simple optics (W. Keene at Raytheon has recently suggested an ingenious technique for avoiding this loss).

In order to improve the S/N it is desirable to rectify and integrate the heterodyne signal over time periods of the order of milliseconds to seconds. The simplest way to do this is to mechanically or electronically chop the incoming signal and use synchronous detection to get the required integration times. Simple chopping systems are no more than 50% efficient. Thus, such a coaxial system has less than 12½% transmission even before absorption losses, modulation losses and other electronic losses are accounted for.

For the values in Figure 1 an additional 25% transmission due to electronic and optical absorption and a quantum efficiency of 20% were assumed, leading to an overall efficiency of 0.6%.

These latter figures are thought to be unduly conservative for current technology. Quantum efficiency of 50% is achievable and it should be possible to achieve a net transmission of 50% through the optics and electronics with careful design. Thus, a more optimistic estimate of the efficiency of a coaxial system would be 3%, (improvement of S/N by factor 5 over values in Ref. 1) with the possibility of extending this to 25% if a way can be found to avoid the beam splitter and chopper losses. If such improvement can be achieved, useful detection ranges for CAT may be possible at moderate powers.

The effect of particle size has also been studied. Very large particles cannot follow the fluctuating fluid velocity whereas very small particles will have a Brownian motion due to the random nature of the molecular impacts superimposed on their mean motion. For normal aerosols (0.1 - 10μ radius) this is not expected to be a problem in the atmosphere. For very small particles (< 100°A radius) the Brownian motion can be appreciable. Although Brownian motion can be distracting in a study of fluid velocity it does provide a means of directly measuring the translational temperature of the gas.

The degradation of the transmitted and returning electromagnetic signal due to atmospheric turbulence is fairly well understood at the present time and fairly good descriptions of laser propagation have been obtained based on the Kolmogoroff theory of isotropic turbulence. Some extension is required for application to short range focused systems. In the present study a small amount of effort has been devoted to improving these models. In particular, for radar scattering from inhomogeneities in the refractive index, the propagation models based on scattering from eddies in the inertial subrange may fail for wavelengths comparable to the inner scale of the turbulence.

For evaluating acoustic propagation and scattering at low altitudes existent theory is adequate. We have reviewed the literature and constructed approximate propagation models in order to evaluate the potential of low altitude acoustic monostatic and bistatic diagnostics in coherent and incoherent systems.

Atmospheric Turbulence

In considering the types of turbulence encountered in the atmosphere we may consider several distinct regions.

1. Low Altitude Turbulence characterized by the earth boundary layer.
2. Clear Air Turbulence which is characterized by undulant and turbulent motions in clear atmosphere away from the atmospheric boundary layer.
3. Cloud and Storm Turbulence.

For the purpose of designing a detection system for the measurement of turbulence in the atmosphere a study of the known characteristics of these regions will be made. Briefly some of the characteristics of these regions are the following.

The atmospheric boundary layer (0-300 meter): It has been found that for stable temperature gradients the turbulence intensity depends on wind speed and terrain roughness but very little on altitude. The average value of low altitude turbulence intensity is approximately 3.0 ft. sec.$^{-1}$. In unstable atmospheres Richardson number effects become important and a simple relationship between turbulence intensity and wind velocity is no longer valid and the intensity given above is altered. Of all three types of turbulence mentioned above

turbulence in the atmospheric boundary layer is the best understood and is relatively well documented.

Clear Air Turbulence (CAT): CAT usually originates from the local shears of winds such as the jet stream. It is usually found in relatively shallow layers. However the extent of the turbulence patches is of the order of tens of miles. Often a turbulence prone layer may be found which extends for hundreds of miles with turbulence patches normally distributed randomly, but sometimes occurring at regular intervals.

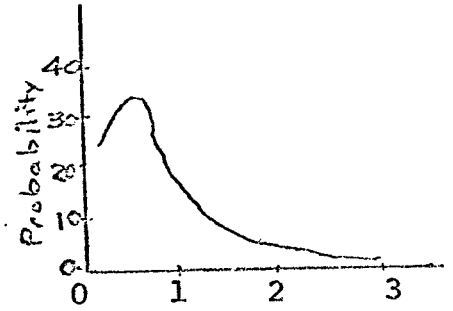

Figure 1.2: Layer Thickness (KFt)

Cloud and Storm Turbulence: In mild storms associated with cumulonimbus clouds it has been indicated that the turbulence may be regarded as a random process. The average value of the vertical component of the turbulence has been found to be of the order of 7-8 ft. sec.$^{-1}$ while the average length of the turbulence patches is of the order of the size of the cloud, several miles. A model of turbulence intensity distribution in cumulonimbus clouds based on flight measurements was proposed by Pinus, Fig. 3. The turbulence intensity from his model which are those evident in a strong storm are about three times as large as those measured above.

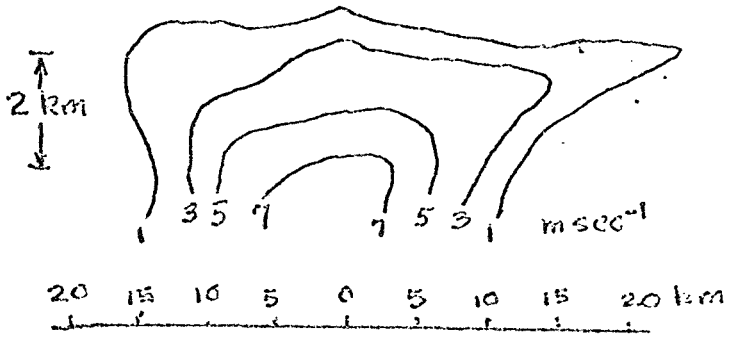

Figure 1.3

Non-Doppler Laser Technique

In the study we have made a brief comparative analysis of various remote sensing techniques for turbulence and wind profile measurements for the particular applications of interest. The techniques which have been considered include:

Radar Doppler backscatter (monostatic)
Radar forward scatter and propagation
Acoustic backscatter
Acoustic refraction and forward scatter

Techniques which remain to be evaluated include:

Scintillation of distant sources
Crossed beam correlations
Passive radiometry
Inversion techniques
Incoherent lidar

The initial studies indicated an appreciable potential for acoustic techniques for low altitude short range applications, and it is intended to expand this portion of the effort.

REFERENCES:

1. "Heterodyne Detection of Monochromatic Light Scattered from a Cloud of Moving Particles," A. Thomson and M.F. Dorian, Convair Report GDC-ERR-AN-1090, June 1967.

2. "Infrared 10.6 Micron Heterodyne Detection with Gigahertz IF Capability," F.R. Arams, E.W. Sard, B.J. Peyton, F.P. Pace, IEEE JQE-3, pp. 484-492, 1967.

3. "Optical Heterodyne Communications Experiments at 10.6μ," F.E. Goodwin and T.A. Nussmeier, IEEE JQE-4, pp. 612-617, 1968.

4. "A High-Power CO_2 Laser Radar Transmitter," P.A. Miles and J.W. Lotus, IEEE JQE-4, pp. 811-819, 1968.

5. "High-Power Single-Mode CO_2 Laser," W.J. Witteman, IEEE JQE-4, pp. 786-788, 1968.

II. Amplitude Modulation due to Finite Aerosol Density

SUMMARY

The frequency spreading effects of amplitude modulation due to convection of aerosols through the coherence volume are discussed. It is shown that the frequency spread due to amplitude modulation is independent of particle density for randomly distributed particles. The spread increases as the coherence volume decreases. For a focused system the frequency spreading for an f/1 system (focal volume dimension of order of a wavelength) is comparable to the Doppler shift and effectively prevents accurate measurement of velocity. This effect limits the spatial resolution that can be achieved by a laser doppler measurement instrument and is important in thin boundary layers. Limiting spatial resolutions are calculated for various applications and geometries.

The present calculations pertain to simple convection along rectilinear trajectories through the coherence volume. More detailed calculations are currently being carried out to extend the analysis to include the effects of particle acceleration and velocity change during transits through the coherence volume.

ANALYSIS

The amplitude modulation induced by convection of the particles through the focal region induces a frequency spreading of the signal and puts a lower limit on the accuracy with which the frequency or velocity can be measured. This is of little consequence in atmospheric application where large focal regions are anticipated. However, for boundary layer studies the constraint may be severe.

In this note we estimate the frequency spreading of the signal due to convection of particles across a finite width beam. Consider the convection at a constant velocity $\vec{v}$ of a system of particles through the focal region of a laser doppler scattering system.

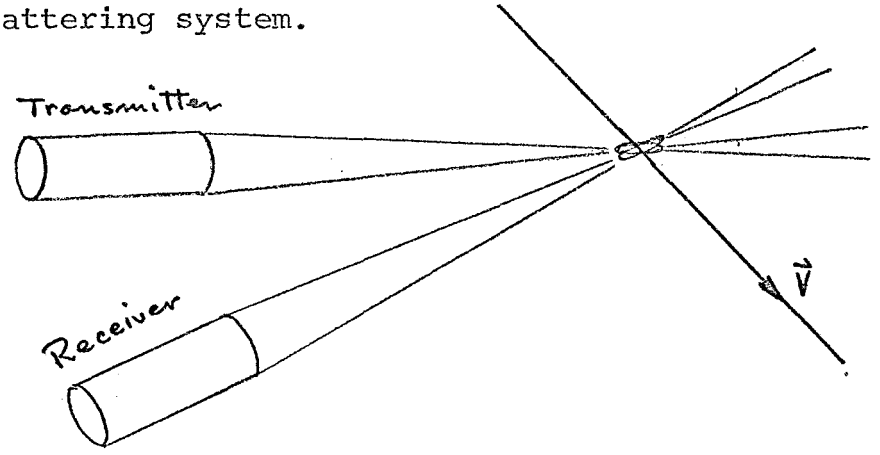

Fig. 2:1.

The amplitude of the backscattered wave is proportional to

$$S(t) \sim \sum_i \left\{ f(\vec{x}_i)\ \sigma_i E_o\ \exp\left[-i\omega_o t + i2\vec{k} \cdot \vec{x}_i \right] \right\} \qquad (2.1)$$

where σ is the back scatter cross section, $f(x)$ describes the beam profile and $\vec{x}_i$ is the instantaneous position of the ith particle. For convection at constant velocity $\vec{v}$

$$\vec{x}_i = \vec{x}_i^o + \vec{v}t \qquad (2.2)$$

Thus, for propagation along the x axis

$$S(t) \sim \sum_i f(\vec{x}_i^o + \vec{v}_\perp t)\ \exp\left[-i(\omega_o t - 2kv_x)t + i2kx_i^o \right] \qquad (2.3)$$

where $\vec{v}_\perp$ is the convection velocity component perpendicular to the beam axis. After heterodyning (with a local oscillator at frequency ω_o) and averaging over optical frequencies the time dependent beat signal is proportional to

$$S'(t) \sim \sum_i f(\vec{x}_i + \vec{v}_\perp t) \exp\left[i2kx_i^o + i2kv \sin\frac{\theta}{2} t\right] \qquad (2.4)$$

where the sum is over all particles.

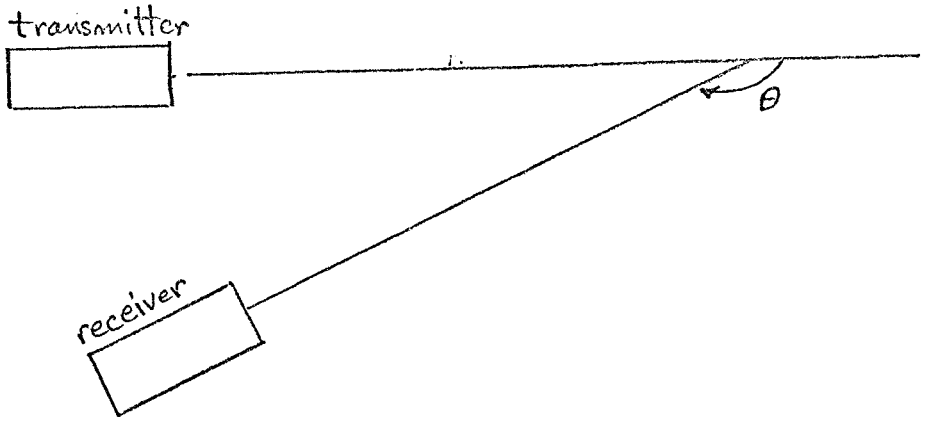

Fig. 2.2: Scattering Geometry.

For a beam having a Gaussian profile:

$$f(x) = \frac{1}{\sqrt{\pi}\Delta} \exp\left[-x^2/\Delta^2\right] \qquad (2.5)$$

the Fourier components of the signal have the form

$$S'_\omega \sim \sum_i \int_{-\infty}^{\infty} \frac{1}{\sqrt{2}\,\pi\Delta} \exp\left[-\frac{(x_i^o + v_\perp t)^2}{\Delta^2} + i\left(2kv \sin\frac{\theta}{2} - \omega\right) t + i2kx_i^o\right] dt$$

$$\sim \sum_i \exp\left[-\left(\frac{x_i^o}{\Delta}\right)^2 + i2kx_i^o - \left[\omega - 2k\bar{V} \sin\frac{\theta}{2} - \frac{2v_\perp x_i^o}{\Delta^2}\right]^2 \left(\frac{\Delta}{2v_\perp}\right)^2\right] \qquad (2.6)$$

Thus, for convection at constant and uniform velocity of a random distribution of aerosols through a gaussian beam the detected heterodyne signal has a mean frequency equal to the Doppler shift:

$$\bar{f} = \bar{\omega}/2\pi = \frac{2v}{\lambda} \sin\theta/2 \qquad \text{Hz} \qquad (2.7)$$

and has a gaussian spectral profile of width (half width at 1/e points) equal to

$$\Delta f = \frac{1}{2\pi}\left(\frac{v_\perp}{\Delta/\sqrt{2}}\right) = \frac{v_\perp}{2\pi\Delta'} \quad \text{Hz} \tag{2.8}$$

Here Δ is the 1/e half width of the amplitude of the beam and $\Delta' = \Delta/\sqrt{2}$ is the 1/e half width of the beam intensity.

The spreading expressed as a fraction of the Doppler shift is (full width between 1/e points divided by $\bar{f}$):

$$\beta = \frac{2\Delta f}{f} = \frac{\lambda}{2\pi\Delta'}\frac{v_\perp}{v}\frac{1}{\sin\theta/2} \tag{2.9}$$

In Table 2:1 we have tabulated the minimum transverse spatial resolution (Δ') allowable in order to achieve a given fractional spreading for the particular case of transverse flow ($v = v_\perp$). For a focused backscatter system the longitudinal spatial resolution is larger than Δ' by a factor of order Δ'/λ (i.e. $\delta \sim \Delta'^2/\lambda$). Thus the value of the minimum longitudinal resolution required to achieve a given value of β is

$$\delta = \frac{\lambda}{[2\pi\beta \sin\theta/2]^2}\left(\frac{v_\perp}{v}\right)^2 \tag{2.10}$$

Table 2.1: Minimum Spatial Resolution (Transverse): for $V = V_{\perp}$

Fractional frequency spread β	$\lambda = 10.6\mu$			$\lambda = 0.5\ \mu$		
	$\theta = 180°$	90°	11°	$\theta = 180°$	90°	11°
0.03	.0056 cm	.0079 cm	.058 cm	.00026 cm	.00037 cm	.0027 cm
0.10	.0017	.0024	.018	.0008	.00011	.00085

Table 2.2: Minimum Spatial Resolution (Longitudinal) for Focused System ($\theta = 180°$ only)

β	$\lambda = 10.6\ \mu$	$\lambda = 0.5\ \mu$
0.03	0.027 cm	0.0013 cm
0.10	0.0027	0.00013 cm

III. DIAGNOSTICS OF THE BACKSCATTER SIGNAL

Typical power spectra for clear air turbulence at high altitude show roughly isotropic character with a Kolmogoroff - 5/3 law for wavelengths less than 10,000 feet. The problem of an appropriate diagnostic measure may be approached as follows. High speed aircraft are sensitive only to wind motions (primarily vertical gust velocities) of wavelengths greater than 2000 to 10,000 feet. Although there is little guarantee that an isotropic model of turbulence applies to high altitude wind motions at long wavelengths (> 10,000 feet), we will use as a model the Von Kármán spectrum

$$E = \frac{2\sigma^2 L}{\pi} \frac{1}{[1 + (1.339Lk)^2]} \qquad (3.1)$$

where the turbulence scale L is expected to be greater than 2000 feet in typical situations

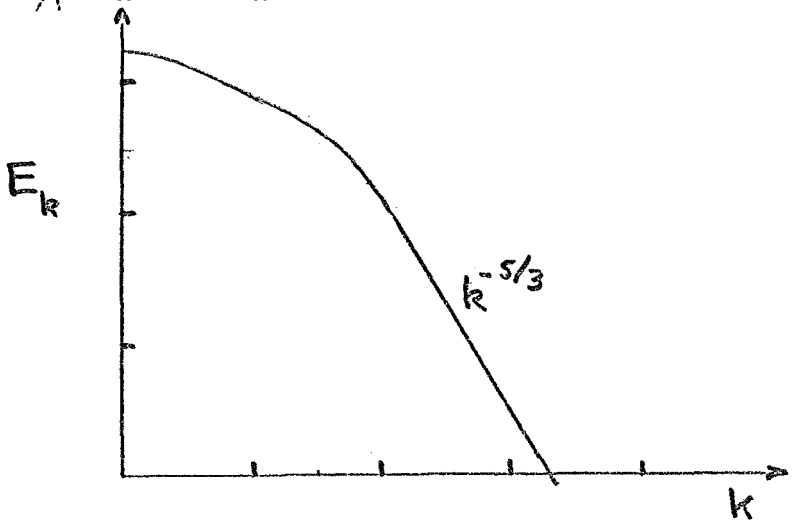

Figure 3.1

and at wave numbers less than $1/(1.339\,L)$ the motion may appear highly anisotropic. For pulse lengths less than 10,000 feet (3 km), it is wavelengths comparable to the pulse length that predominantly determine the frequency spreading of the signal.

Ignoring for the moment the spread in the signal due to the finite time duration of the pulse we would expect a

frequency distribution determined as follows. If we assume a Gaussian shape the signal has the spectral form

$$D(f) = \frac{1}{\sqrt{\pi}\,\Delta} \exp\left(-(f-\bar{f})^2/\Delta^2\right) \tag{3.2}$$

where

$$\Delta = 2\bar{V}/\lambda$$

$$\simeq \frac{2}{\lambda}\sqrt{E(k_o)\,k_o} \tag{3.3}$$

and k_o is of order of the inverse of the pulse length. Thus for the Von Kármán spectrum

$$\Delta \sim \frac{2\sigma}{\lambda}\sqrt{\frac{2}{\pi}}\,\frac{(L/\ell)^{\frac{1}{2}}}{\left(1 + (1.339L/\ell)^2\right)^{5/12}} \tag{3.4}$$

$$\simeq 2\sqrt{\frac{2}{\pi}}\;\frac{\sigma}{\lambda}\;\frac{1}{(1.339)^{5/6}}\;(\ell/L)^{1/3} \quad \text{for } \ell \ll L$$

Since a gaussian spectrum is expected there are only two parameters of measurable interest: Δ and $\bar{f}$ and it appears appropriate to design instrumentation which directly senses these quantities.

The spectral spreading by amplitude modulation is of order C/ℓ

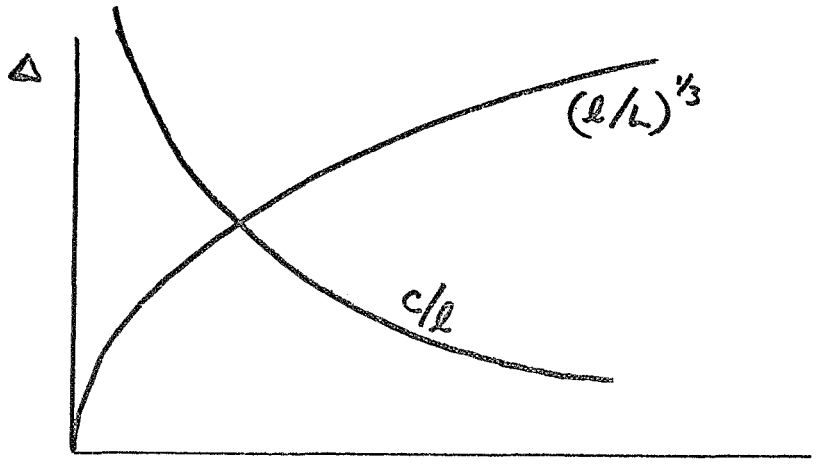

Figure 3.2

In order that the spread be dominated by turbulent motion

$$\frac{\lambda c}{\sigma L} < 2\sqrt{\frac{2}{\pi}} \frac{\sqrt{\ell/L}}{\left(1 + \left(\frac{1.339L}{\ell}\right)^2\right)^{5/12}} \tag{3.5}$$

or

$$\frac{\lambda c}{\sigma L} < \frac{2\sqrt{\frac{2}{\pi}}}{(1.339)^{5/6}} \left(\frac{\ell}{L}\right)^{4/3} \quad \text{for } \ell \leq L \, . \tag{3.6}$$

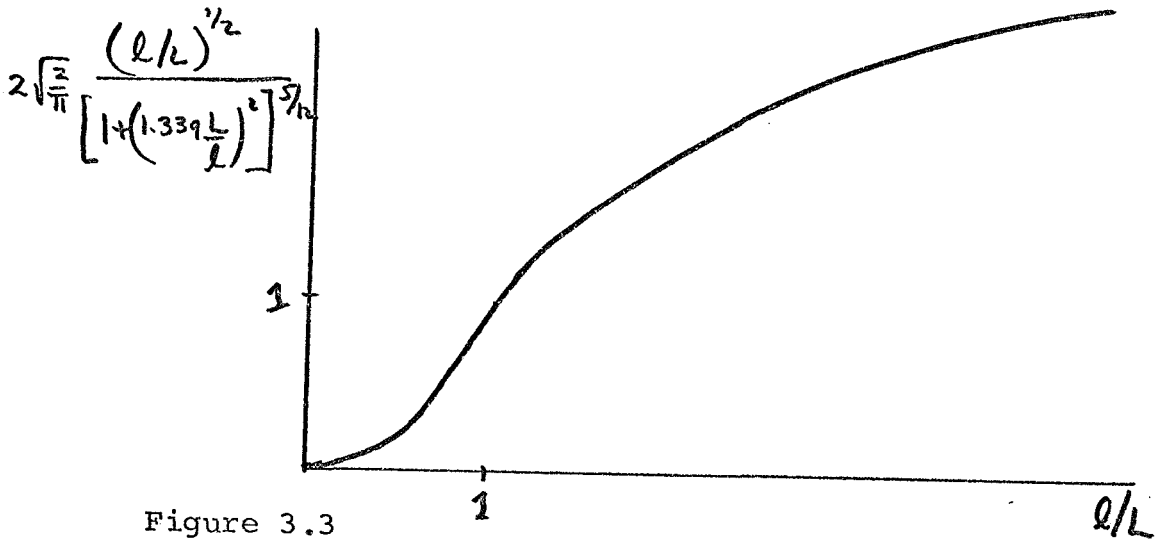

Figure 3.3

Since we cannot consider pulse lengths > L this establishes a lower limit to the measurable velocity spread, i.e. for a measurement

$$\sigma \geq \frac{\lambda c}{L} \tag{3.7}$$

For L = 1 km, $\lambda = 10^{-5}$ m

$$\sigma \geq \frac{10^{-5} \times 3 \times 10^8}{10^3} = 3 \text{ meters/sec} \tag{3.8}$$

and this lower limit can only be achieved by using long pulses.

Since the spectral width increases as $1/\ell$ due to amplitude modulation the pulse width should be shown as long as possible consistent with the spatial resolution required. Fortunately this favors signal to noise when the peak power is limited.

Since the shape of the spectral distribution is not expected to contain significant information other than width (which will be a mixture of doppler spread and amplitude modulation spread) more useful data may be accessible by ignoring spectral width and simply measuring mean frequency (mean velocity) in the pulse as a function of range. Essentially by definition the spectral width of the signal is always comparable to or smaller than the expected value of the displacement of the mean frequency. It is the mean velocity averaged over the pulse and its variation in space that contains the Kolmogoroff or non-Kolmogoroff spectrum information. Also if it were the vertical wind velocity that were being measured this is directly what is desired for the aircraft. On board instrumentation cannot measure lateral velocities and therefore must depend on theory to relate longitudinal velocity to the other components.

It is recommended therefore that consideration be given to a system which simply measures mean velocity or frequency shift averaged over pulse length and obtains this as a function of range. By offsetting the frequency by the aircraft wind speed a two dimensional sweep display is possible with range and angle as coordinates and intensity proportional to pulse averaged velocity difference from a reference. Intensity

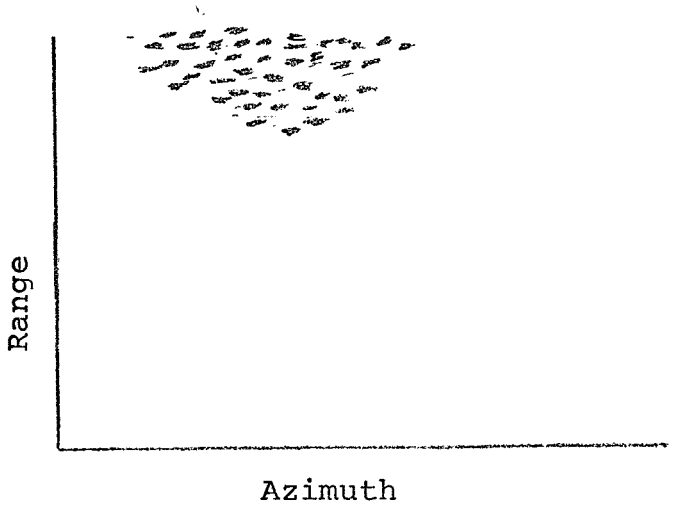

Fig. 3.4

gradients then imply velocity shear and zero or uniform intensity implies uniform atmosphere.

Since filter bank systems are apparently available at relatively low cost in sets containing up to 100 individual filters, the question of whether to use analogue (liner FM discriminators) or digital techniques (filter banks) to record the mean velocities and widths is mainly one of signal to noise calibration and instrument drift, etc. Digital techniques (according to Raytheon) are considerably better at low signal to noise levels than are analogue techniques and are favored for the present system.

IV. FEASIBILITY STUDY OF DETECTION OF STRATOSPHERIC MOTION BY A GROUND BASED 10.6μ LASER DOPPLER DETECTION SYSTEM

Summary

There are presently under consideration coherent laser detection systems designed to detect atmospheric turbulence at or near the tropopause from an airborne platform. In order to obtain the requisite design information for sugh a measurement program it would appear desirable to conduct preliminary measurements from the ground since the achievable signal to noise raio in a ground system is at least as good and probably greater than for an airborne system under selected meteorological conditions.

The advantages of a ground based measurement as compared to an airborne measurement are several and include:

1) Availability of larger useful apertures (diameter of 2 feet or greater as compared to a probable 1 ft.-aperture for an airborne system) resulting in an enhancement of S/N at a given range by about 6 db.

2) Availability of a relatively controlled laboratory environment for optics-laser-detectors and electronics.

3) Space and power limitations are not severe.

4) Stability of line of sight in space.

5) Ability to take extended and repeated measurements under variety of conditions. Experiments can be repeated at relatively low cost.

6) Ability to make extensive use of pulse integration techniques.

7) Ability to utilize bread board laser and electronic instrumentation.

In order to be able to utilize effectively an aperture of 50 cm diameter at 10.6μ, the average value of the refractive index structure constant should be less than about 10^{-8} $cm^{-1/3}$ for a near vertical path. This constraint may restrict the measurement to night time operation or to periods of good seeing conditions during the day. In Table I we have tabulated a set of parameters for such a measurement. The value of the back scattering parameter is not certain at 10.6μ for altitudes of the order of 10 km but present estimates indicate likely values in the range $10^{-6} - 10^{-7}$ km^{-1} $ster^{-1}$ with the higher value being more consistent with recent estimates of upper atmosphere aerosol densities. For a pulsed system operating in the far field region of the optics, the signal to noise ratio is

$$S/N \sim \eta \frac{J}{h\nu} \overline{n\sigma}\, c\tau\, D^2/R^2 \qquad (4.1)$$

where J is the net output energy in the observation time, τ the pulse duration, D the aperture diameter, and R the range. In Table I we have assumed an overall optics-detector-electronics efficiency η of 10 per cent. (Values given in parentheses correspond to η = 1%). Theoretically it should be possible in a pulsed system to achieve efficiencies approaching the detector quantum efficiency (30-50%). However, for design purposes, it may well prove advantageous to be somewhat pessimistic in the choice of overall efficiency.

TABLE 4.1

Expected Signal/Noise for a Possible Ground Based Measurement

Aperture	:	50 cm
Low Altitude Atmospheric Turbulence	:	$c_n < 10^{-8}$ cm$^{-1/3}$
Detection Altitude	:	10 km
Look Angle	:	vertical ± 45°
Round trip delay time	:	70 μsec
Pulse length	:	2 μsec
$\overline{n\sigma}$	:	$10^{-6} - 10^{-7}$ km^{-1} - ster^{-1}
Scattering and absorption losses	:	3 db
Assumed optics-detector-electronics efficiency (η)	:	0.1 (.01)

Signal to Noise Ratio Per Pulse*

Pulse energy	$\overline{n\sigma} = 10^{-6}$ km^{-1} ster^{-1}	$\overline{n\sigma} = 10^{-7}$
20 mj	80 (8)	8 (0.8)
200 mj	800 (8)	80 (8)

Signal to Noise after integrating for one second at 600 pps

Pulse energy	Mean power	$\overline{n\sigma} = 10^{-6}$km^{-1}ster^{-1}	$\overline{n\sigma} = 10^{-7}$
20 mj	12 watts	48,000 (4,800)	4800 (480)
200 mj	120 watts	480,000 (48,000)	48,000 (4800)

Incoherent Integration

Pulse energy	Mean power	$\overline{n\sigma} = 10^{-6}$km^{-1}ster^{-1}	$\overline{n\sigma} = 10^{-7}$
20 mj	12 watts	2000 (200)	200 (20
200 mj	120 watts	20000 (2000)	2000 (200)

*Values in parentheses correspond to $\eta = 0.01$

Reference to Table 4.1 indicates that with a laser capable of producing 100 millijoule pulses with peak powers of 100 kw, it should be possible to achieve a measurable signal with one pulse using a wide frequency bandwidth.

Two modes of operation may be envisaged, one where the line of sight is fixed in space and the returning signal is spectrally analyzed or filtered to yield the distribution of velocities in the scattering medium, and another mode which requires measuring only the mean frequency offset or mean velocity of particles in the coherence volume and presenting this data as a function of range and angular inclination of the line of sight. This latter mode of presentation has the advantage of allowing presentation of the local mean velocity as a function of range and elevation angle while only being about 3 db in signal/noise below the full bandwidth signal. This latter mode would be particularly appropriate when coupled to simultaneous measurements of high altitude radar backscatter such as can be obtained with the high power radars. In Table II we present comparative data for the Wallops Island radars and for the laser system described above.

TABLE 4.2

Comparison of Signal/Noise per pulse for Ground Based Laser and Radar Detection at 10 km altitude

System Characteristics

Wallops Island Radars			10.6μ Coherent Laser
	Pulse energy	Resolution	Pulse energy : 200 mj Pulse length : 2μsec Aperture : 50 cm Efficiency : $\eta = 0.05$ Absorption loss : 3 db
UHF	6 joules	150 m	
S band	3	150 m	
X band	1.8	300 m	

Signal/Noise Ratio per pulse

Radar			
C_n^2	S/N		
	UHF	S	X
$10^{-16} cm^{-2/3}$	4200	700	50
10^{-18}	42	7	0.5

CO_2 Laser		
$n\sigma(10.6\mu)$	(S/N) total	(S/N) mean velocity measurement
$10^{-6} km^{-1} ster^{-1}$	400	200
$10^{-7} km^{-1} ster^{-1}$	40	20

Since the laser system provides a measurement of the mean velocity parallel to the line of sight in the coherence volume (or, by time differentiation, its gradient: $dV_{\|}/dr$), and the radar detects the rms refractive index fluctuations, simultaneous measurements at comparable sensitivities of scattering from the upper atmosphere can be expected to be a fruitful source of information on atmospheric motion and turbulence. A laser system such as the one described cannot be considered as an operational tool for detection of high altitude CAT on a routine basis because of the constraints of clear weather and good seeing conditions. However, as a research tool, it appears to offer considerable promise if an overall efficiency factor of 5% can actually be achieved and if the backscattering conditions at 10.6μ are as high as assumed here.

Effect of Elevation Angle

An upward looking laser backscatter system of the type discussed detects the mean vertical velocity in a coherence volume which has lateral dimensions of the order $\frac{\lambda}{D}R \simeq 20$ cm and a length $c\tau \simeq 300$ m. The major difference between a ground based measurement and an airborne measurement is the velocity component detected. Simultaneous measurement of the same volume by two ground systems separated by a few kilometers would provide both the horizontal and vertical velocity components. Large ground separations are required since small velocity and frequency differences are distorted by amplitude modulations induced by the short pulse length.

The Doppler frequency offset in a ground based system is small and some method for isolating the receiver from scattered radiation from the transmitter is required. For a range

of 10 km the round trip line is $2 \times 10^6/3 \times 10^{10} = 70\mu$sec. A mechanical shutter can easily operate in this time, i.e. a disk rotating at 600 rps and having diameter of 4 cm has peripheral speed π (600) = 7200 cm/sec. In 50μsec a slot at the edge moves $7200 \times 50 \times 10^{-6}$ cm = 0.36 cm = 3.6 mm. Thus, by focusing the beam to a small spot on such a switch and synchronizing the transmitter, the transmitter feed through can be strongly blocked. Two such switches could be used to eliminate virtually all feed through.

V. TWO PHASE FLOW EFFECTS

The mean motion of a finite sized particle in a time varying fluid bath can be approximated by a relaxation equation of the form

$$\frac{dV}{dt} = - \frac{C_D \rho (V_f - V)^2 \pi r^2}{2m} \tag{5.1}$$

where m and r are the particle mass and radius respectively, C_D its effective drag coefficient and V_f the fluid mean velocity in the neighborhood of the particle. For large particles ($r >> \lambda$ where λ is the mean free path in the fluid)

$$C_D \simeq \frac{24}{R_e} = \frac{24 \mu}{\rho (V_f - V) r} \tag{5.2}$$

where μ is the fluid viscosity. Thus

$$\frac{dV}{dt} = \frac{12 \pi r \mu (V_f - V)}{m} \quad . \tag{5.3}$$

For spherical particles of bulk density ρ_p

$$\frac{dV}{dt} = \frac{9\mu}{\rho_p r^2} (V_f - V) = \frac{V_f - V}{\tau} \tag{5.4}$$

and the particle velocity history is given by

$$V(t) = \int_{-\infty}^{t} V_f(t') \exp \left[- \int_{t'}^{t} dt''/\tau \right] \frac{dt'}{\tau} \tag{5.5}$$

Here τ is the characteristic relaxation time:

$$\tau = \frac{\rho_p r^2}{9\mu} \tag{5.6}$$

Using the simple kinetic theory expression for μ ($\mu = \rho\bar{v}\lambda/3$ where $\bar{v}$ is the arithmetic mean velocity in the fluid) we may write approximately

$$\tau = \frac{1}{3} \frac{\rho_p}{\rho} \frac{r^2}{\bar{v}\lambda} . \tag{5.7}$$

In the limit of small particle radius ($r << \lambda$) the relaxation time has the form

$$\tau = \frac{2}{3} \frac{\rho_{pr}}{\rho \bar{v}} \xi \tag{5.8}$$

where ξ is a measure of the momentum accommodation coefficient. A useful interpolation expression can be formed from these two limits:

$$\tau \approx \frac{2}{3} \frac{\rho_p}{\rho} \frac{r}{\bar{v}} \left(\xi + \frac{r}{2\lambda}\right) \tag{5.9}$$

Referencing the parameters to those of air at STP and 1μ radius particles of density 2 qm/cm^3, we may write

$$\tau = 3.2 \times 10^{-6} \left(\frac{\rho_p}{2}\right) \left(\frac{10^{-3}}{\rho}\right) \left(\frac{r}{1\mu}\right) \left(\frac{4 \times 10^4}{\bar{v}}\right) \left[\xi + 2.5 \left(\frac{r}{1\mu}\right)\left(\frac{0.2\mu}{\lambda}\right)\right] \text{secs.} \tag{5.10}$$

TABLE 5.1

r	$\rho = 10^{-3}$, $\xi = 1$ τ ($\lambda = 0.2\mu$)	$\rho = 10^{-4}$, $\lambda = 2\mu$ $\xi = 1$	$f = \frac{\omega^*}{2\pi} = \frac{1}{2\pi\tau}$
1μ	8 μsec	2 = 32 μsec	20 kHz
3μ	80	200	2 kHz
10μ	800	800	0.2 kHz

Particle Motion in a Sound Wave

When $V_f(t)$ is harmonic

$$V_f(t) = V_o e^{i\omega t} \tag{5.11}$$

the particle velocity is given by the expression

$$V(t) = \frac{V_o}{1 + i\omega\tau} e^{i\omega t} = \frac{V_f(t)}{1 + i\omega\tau} \tag{5.12}$$

and the rms particle velocity is less than the fluid velocity by the factor $(1 + \omega^2\tau^2)^{-\frac{1}{2}}$. In terms of the power of the acoustic wave

$$P = \frac{P_a}{2C} \overline{V_f^2} = \frac{\rho_a c}{2\gamma} \overline{V_f^2} \tag{5.13}$$

where P_a is the ambient pressure and C the sound velocity, the particle rms velocity is given by

$$V_{rms} = \left(\frac{2CP}{P_a}\right)^{\frac{1}{2}} (1 + \omega^2\tau^2)^{-\frac{1}{2}}$$

$$= 8\left[\left(\frac{1\text{ atm}}{P_a}\right)\left(\frac{C}{300\text{ m/s}}\right)\left(\frac{P}{1\text{ w/m}^2}\right)\right]^{\frac{1}{2}} \left[1 + \omega^2\tau^2\right]^{-\frac{1}{2}} \text{ cm/sec.} \tag{5.14}$$

At high frequencies ($\omega\tau > 1$), the particle velocity for large particles at STP is given by

$$V_{rms} = 160\sqrt{\frac{P}{1\text{ w/m}^2}} \left(\frac{1\mu}{r}\right)^2 \left(\frac{1\text{ kHz}}{f}\right) \text{ cm/sec.} \tag{5.15}$$

Because of the dependence of velocity on radius a cloud of particles of varying size distribution will experience streaming of smaller particles past larger particles and an

enhancement of the coagulation rate. The normal coagulation process is associated with Brownian motion. The velocities involved in this latter case are, in equilibrium, of order

$$\overline{V}_{Brownian} \approx \sqrt{3\,kT/m}$$

$$\approx \sqrt{\frac{9\,kT}{4\pi\rho_p}} \quad \frac{1}{r^{3/2}} \tag{5.16}$$

at 273°K and for $\rho_p = 2$ qm/cm^3

$$V_{Brownian} = 0.1(1\mu/r)^{3/2} \text{ cm/sec} \tag{5.17}$$

TABLE 5.2

r	$V_{Brownian}$	V(P = 1 w/m^2; 1 kHz
0.1μ	3.0 cm/sec	8 cm/sec
1μ	0.1	8
3μ	0.02	8
10μ	0.003	1.6

VI. DETECTION OF AIRCRAFT TRAILING VORTICES

Vortex Structure and Dynamics

The wrap up of the vorticity into two well-defined trailing vortices shed from the wings of a finite aspect ratio aircraft is fairly well understood. The downward momentum given by the aircraft to the air passed over generates two trailing vortices which move downward under their mutual influence. When viscous and turbulent effects can be neglected the interaction of the ground can be interpreted in terms of image vortices which cause the trailing vortices to arrest their downward motion and to move horizontally away from the track of the aircraft maintaining a constant altitude. The circulation of the vortices is proportional to the lift per unit span divided by the aircraft speed. The drag (viscous and induced) of the aircraft and the thrust of the propellors or jets determine the axial motion that appears in the vortices, particularly in the core. The details of the velocity distributions and of the decay and breakup phenomena are less well understood. Hoffman and Joubert have developed a theory for fully turbulent vortices which appears to predict the radial distribution of tangential velocity fairly well, except in the core region and at very large radii (McCormick et al.). Here the fully turbulent model and neglect of axial and radial convection of tangential momentum leads to a self-preserving distribution in which the circulation increases logarithmically with radius. However, the dimensions of the core, and the strong axial velocities that are evident in the NASA smoke visualization studies are not predicted by this theory. It is possible that disappearance of this structure is associated

with the phenomenon of vortex breakdown which has been observed in a number of laboratory experiments.

Induced Aircraft Rolling Moments

The sensitivity of the roll moment induced in an aircraft flying through a vortex wake to the details of the velocity distribution in the vortex can be roughly modelled as follows. We consider an aircraft flying parallel to a line vortex whose axis intersects the aircraft wing at a distance x_o from the aircraft axis. We assume that the vortex tangential velocity structure can be modelled according to

$$V = \frac{\Gamma}{2\pi}\frac{r}{a} \qquad \text{for } r < a$$
$$= \frac{\Gamma}{2\pi}\frac{r}{a} \qquad \text{for } r > a \tag{6.1}$$

where r is the distance from the vortex axis. The local increment in angle of attack is directly proportional to the vortex tangential velocity and the induced rolling moment takes the form

$$M \sim C_1 \int_{-b}^{b} V x \, dx \tag{6.2}$$

where C_1 is a constant.

In order to get an explicit expression for M consider only the case where the wing extends entirely through the vortex core (i.e., $\frac{b}{2} > X_o + a$). In this case the induced rolling moment for a large aspect ratio wind is proportional to

$$M \sim \text{(constant)}\ \frac{\Gamma b}{2\pi}\left\{1 - \frac{4a}{3b} + \frac{x_o}{2b}\,\ell n\left(\frac{a}{x_o}\,\frac{b - 2x_o}{b + 2x_o}\right)\right\}. \tag{6.3}$$

The moment is maximum for a vortex centered on the aircraft line of flight:

$$M_{max} = (\text{constant}) \frac{\Gamma b}{2\pi} \left(1 - \frac{4a}{3b}\right) \quad . \qquad (6.4)$$

Thus until the vortex core diameter exceeds about one half the semi (effective) wing span (b/2) the rolling moment is greater than 67% of the value for a line vortex.

These estimates indicate that, until the core diameter grows to a value of the order of half the wing span, the induced rolling moment is insensitive to the details of the radial distribution of vorticity in the vortex.

The empirical correlations of McCormick et al. give, for a large "jumbo" jet for which the circulation is of order 9000 ft^2/sec, a time dependence for the peak tangential velocity of

$$V_{max}(t) \sim 55 \left(\frac{5\,min}{t}\right)^{\frac{1}{2}} \text{ ft/sec} \qquad (6.5)$$

where t is the time after passage (in minutes). For the simple solid body core rotation described by Equation , this corresponds to a core radius given by

$$a = \frac{\Gamma}{2\pi V_{max}} \sim 25(t/5\,min)^{\frac{1}{2}} \text{ feet.} \qquad (6.6)$$

Since the (semi) wing span of large aircraft are typically about 50 to 100 ft, we thus expect that, for times less than 5 minutes, the induced rolling moments experienced by an aircraft will be insensitive to the details of the diffusion processes within the vortex and can be estimated using an

inviscid line vortex model. Consequently, the application of these empirical vortex decay models implies that the rolling moment experienced by a large aircraft (b > 100 feet) flying along one of the trailing vortices of a "jumbo" jet will be independent of time up to five minutes after the passage of the first jet.

However, it is probably unlikely that these empirical correlations, which were deduced from measurements made with light aircraft, are really applicable to the decay of heavy jet aircraft wakes. The interaction of the vortex with its partner or its ground image results in an instability whose characteristic growth time is proportional to b^3/W (see Section). This growth time is much shorter for heavy jet aircraft than for light observation aircraft. Typical predicted e-folding times are of the order of 20-30 seconds and observed times at altitude for full development of the instability are of the order of 40 to 80 seconds. Since these predicted times are considerably shorter than those required for the vortices to decay by normal diffusion, it should be possible to develop reasonable models for the vortex motion by ignoring the internal diffusion processes and concentrating on the mutual instabilities, the viscous interaction with the ground plane and the effect of ambient wind shear.

Detection Techniques

Among the methods that can be considered for detecting the presence and the structure of trailing vortices are: visualization techniques--smoke emitted from low towers or from wing tip mounted smoke bombs, measurement of ground surface or near surface pressure and wind velocities, laser

doppler backscatter from natural aerosols, acoustic backscatter or forward-scatter techniques, and measurement of vertical temperature gradients. In the following section we will briefly discuss some of these techniques. For the purposes of this discussion it is worth noting that two quantities are of interest: the location of the vortex axis and the radial distribution of the tangential and axial velocity profiles (in particular of the peak velocities). It is expected that the peak axial velocities and peak tangential velocities will be comparable. However, from the point of view of rolling moment induced in unsuspecting aircraft, the tangential velocity is probably more important. Measuring techniques that sense the velocity at some distance from the vortex core yield information on the existence and location of the vortex and on its strength but tell little about the peak velocities that may exist near the core. To detect the phenomena of vortex breakdown, either sensing of the core region itself or else application of a theory that can relate the decay and breakdown processes to the dynamics of the surrounding environment is required.

VII. EXPECTED SIGNAL-TO-NOISE RATIOS FOR A FOCUSED LASER DOPPLER AIRPORT SCANNING SYSTEM.

At short ranges the signal-to-noise that can be achieved with a heterodyne measurement of coherent light scattered from atmospheric aerosols is limited primarily by the volume of atmosphere which can be effectively heterodyned. Siegmann (1966) has shown that this latter volume is such that S/N cannot exceed $\eta N \overline{n\sigma} \lambda/4$ where N is the number of photons transmitted in the dwell time, η the overall system efficiency including detector, optics and electronics, $\overline{n\sigma}$ the effective mean value of the product of particle density and backscatter cross section and λ the wavelength. At short ranges such that the scattering point is within the Fresnel region of the optics this upper limit can be achieved only by focusing the transmitter and receiver on a common volume and by bringing the optic axes of the two systems into coincidence. Fortunately, such a coaxial system has a number of practical advantages, including the requirement for only one set of optics for each velocity component required, and minimum sensitivity to alignment errors and to vibration. The major disadvantage of a focused system lies in the resolution range that can be achieved. Since, at short ranges, pulsed systems with pulse lengths short enough to produce the range resolutions required for detection of aircraft wake structures strongly broaden the return infrequency, a CW system is indicated, at least at CO_2 wavelengths (see appendix to this section). Although, in a coaxial focused system, energy scattered from any point along the line of sight can reach the detector and produce a heterodyne signal, efficient heterodyning is only achieved by scattering from a region near the focal point. Effectively the wave scattered

from particles far distant from the focal volume has a spherical wavefront at a point in the receiver where the wavefronts of the local oscillator are plane. This effect leads to very finely spaced interference fringes and results in a low amplitude beat frequency as this fringe pattern sweeps across the detector. The response function for scattering centers located at different distances from the focal volume is shown in Figure . Except for a numerical factor the distance between half power points is proportional to $\lambda L^2/D^2$ where D is the aperture and L the range.

To demonstrate the problems imposed by scanning requirement estimates have been carried out for a particular configuration. Here it was decided to scan a segment of a vertical plane normal to the vortex axis up to an elevation angle of 10° and to be able to achieve good signal to noise and adequate spatial resolution at ranges 200 meters and 1200 (see figure). A coaxial CW CO_2 laser system was considered with an aperture of 50 cm. The axial resolution of such a system is about 20 meters (half power response) at the nominal range of 500 m and changes to 3.3 m at minimum range and 177 m at maximum range. The diameter of the focal volume is 1.4 cm nominal and is 0.4 cm minimum and 2.8 cm maximum. The scanning mechanics were required to be able to scan the vertical plane so as to divide the range into 60 range cells and the integration time during the lateral scan required to be such as to yield an angular resolution of 1 meter at a range of 500 meters. For a two-second frame time this system allows 3000 data points per second (corresponding to a dwell time on each resolution element of 300μ seconds).

Since the axial resolution achieved by this system is larger than the expected dimensions of the high velocity region in the vortex core, only part of the returned signal will be associated with the core region. The signal to noise due to scatter from the core region (of dimension ℓ_c) is therefore to be reduced by the factor $\ell_c/\Delta\ell_f$ where $\Delta\ell_f$ is the depth of field. For a value of $\overline{n\sigma}$ at 10.6μ equal to 0.8×10^{-3} km^{-1} (based on a model for clean continental air at sea level) a mean laser output of 10 watts and an overall system efficiency of 1%, the signal to noise is estimated to be of order 150 per meter length in the coherence volume at a range of 500 meters.

At the maximum range of 1200 m the signal to noise due to the vortex core region is of order 25 per meter. Although uncertainties exist concerning values of $\overline{n\sigma}$ that actually occur, the present estimates appear encouraging even in clear air. It is to be expected that when the visibility is limited due to particulate matter in the low atmosphere, the backscatter cross section will be greater than that we have assumed here. Of course under conditions of very poor visibility (fog, heavy rain, or snow), the attenuation of the backscattered signal may prevent reliable detection.

Surface Pressure Measurement

When the induced velocities at the ground surface are comparable to the normal winds at the ground, these velocities may be detected using anemometers. An array of pressure transducers may be used under these conditions to follow the track of the vortex across the area of prime concern. Such a detection method may be of limited utility when the vortices are weak or when strong ground winds are present but

may be utilized as a research tool in relatively calm conditions. Also since the pressure at the ground depends only on the net circulation around the vortex it does not reflect information concerning the breakdown of the core or of the peak velocities existent in the aircraft wake.

When the vortices have stabilized with altitude above the ground and are moving laterally under the influence of their images, the velocity (in the inviscid approximation) at the ground surface immediately under the core of the vortex is (neglecting the contribution of the distant counter-rotating image pair

$$V \approx \Gamma/\pi h \qquad (7.1)$$

where Γ is the vortex circulation and h the altitude of the vortex core. For trailing vortices typical of a very large jet ($W \approx 700{,}000$ lbs, wing span ≈ 200 ft) travelling at a velocity of 200 ft/sec, the circulation is of order 9000 ft^2/sec and, for a vortex moving horizontally at an altitude of 100 feet, the induced air velocity at the ground surface is of order 30 ft/sec (the vortex itself translates laterally in calm wind at about 7.5 ft/sec). Although the boundary layer at the ground surface suppresses the velocity close to the ground, the pressure decrement will be significant:

$$\Delta p \sim -\rho v_g^2 \qquad (7.2)$$

i.e. about 0.8 millibars (0.024 in Hg). Such pressures are measurable with relatively crude instrumentation and use of an array of pressure probes at the ground surface would appear feasible under calm wind conditions.

CW versus Pulsed Systems at Short Ranges

For a single pulse system the band width Δf of the transmitted pulse is of the order $1/\tau$ where τ is the pulse duration. In order that this width be less than the local wind velocity (for which $\Delta f = 2v/\lambda$) pulse lengths greater than $\lambda/2v$ are required corresponding to spatial resolutions $\Delta r = c\tau/2$ greater than $c\lambda/4v$. For a CO_2 laser with a velocity resolution of 1 meter/sec. the range resolution $\Delta r \geq 750$ meters. Even for $v = 10$ meters/sec, the range resolution is limited to 75 meters according to this criterion ($\tau = 0.5$ μsec).

If the output shape were precisely known and if the signal to noise ratio is sufficiently large, it should be possible to measure wind velocities which give rise to Doppler shifts smaller than the frequency width of the transmitted pulse. However, since techniques capable of measuring Doppler shifts significantly smaller than the inverse width of the output pulse require high values of S/N and precise knowledge of the output pulse shape it is probable that the effective limit on the velocity detection is still of the order $c\lambda/4\Delta r$.

Thus, for short range applications (ranges of the order of 500 meters or less) a CW system appears necessary at CO_2 wavelengths.

In the visible, a pulsed system may be appropriate for some applications. For example, for a range resolution of order of 10 meters, the minimum detectable velocity at 0.5μ wavelength is about 4 m/sec and requires a pulse duration of 0.07 μsec. However, the reduced effective aperture at such wavelengths during daytime and the lower S/N per joule

available will require a considerably higher output power for the system.

VIII. ACOUSTIC SCATTERING FROM TURBULENT AIRCRAFT WAKES

For a Kolmogoroff spectrum of turbulence the differential acoustic scattering cross section per unit volume per unit solid angle is*

$$\frac{d\sigma}{\sigma\Omega} = 0.03\left(\frac{2\pi}{\lambda}\right)^{1/3}\cos^2\theta\left[\left(\frac{C_v}{c}\right)^2\cos^2\frac{\theta}{2} + 0.13\left(\frac{C_T}{T}\right)^2\right]\left(\sin\frac{\theta}{2}\right)^{-11/3} \tag{8.1}$$

where θ is the scattering angle and C_v and C_T are the velocity and temperature structure coefficients, defined according to:

$$\overline{\left|\vec{v}(\vec{x}+\vec{r}) - \vec{v}(\vec{x})\right|^2} = C_v^2\, r^{2/3} \tag{8.2}$$

$$\overline{\left|T(\vec{x}+\vec{r}) - T(\vec{x})\right|^2} = C_T^2\, r^{2/3}\,. \tag{8.3}$$

The ambient sound speed and temperature are c and T respectively.

In the present estimates we will consider values of C_v^2/c^2 between 10^{-6} and 10^{-8} $cm^{-2/3}$ and $(C_T/T)^2$ between 10^{-5} and 10^{-7}. We have, at 10^3 Hz (λ = 30 cm)

$$\frac{d\sigma}{d\Omega} = 1.7\times10^{-8}\cos^2\theta\left[\left(\frac{C_v/c}{10^{-3}}\right)^2\cos^2\frac{\theta}{2} + 0.13\left(\frac{C_T/T}{10^{-3}}\right)^2\right]\left(\sin\frac{\theta}{2}\right)^{-11/3} cm^2/cm^3. \tag{8.4}$$

---

*For reference purposes it is useful to note that at backscatter ($\theta = \pi$) and for $2\pi R/\lambda >> 1$ the backscattering cross section efficiency from a spherical volume having a temperature difference from ambient of ΔT yields a reflectivity $0.005\,(\Delta T/T)^2$ $ster^{-1}$ whereas for a random scatter

The detectable power scattered into a receiver at a distance R from the scattering region is given by (in the far field)

$$P_r = (P_\tau)_{trans.} \frac{c}{2} \frac{d\sigma}{d\Omega} \frac{A_{rec}}{R^2} \xi \qquad (8.6)$$

where τ is the pulse length, ξ is a factor accounting for the various losses, and P_r is the echo power received per transmitter pulse. In order to achieve a 3 meter distance resolution the pulse length τ should be about 10 milliseconds.

It is convenient to express the signal/noise in terms of a reference system. We choose the following parameters for such a system:

TABLE 8.1

P_τ = 100 watts in 10^{-2} seconds = 1 joule

A_{rec} = 10 m^2

R = 500 m

λ = 0.3 m

$\frac{C_v}{C}$ = 10^{-3} $cm^{-1/3}$ or $\frac{C_T}{T} = 3 \times 10^{-3}$

$$\frac{1}{\pi R^2} \left(\frac{d\sigma}{d\Omega}\right)_{random} = 0.005 \left(\frac{2\pi R}{\lambda}\right)^{1/3} \left(\frac{C_T R^{1/3}}{T}\right)^2 \text{ ster}^{-1}. \qquad (8.5)$$

Here $(C_T R^{1/3}/T)^2$ is a measure of mean square temperature fluctuation $(\Delta T/T)^2$ in such a random medium. Thus the scatter from a volume of turbulent atmosphere is larger than that from a homogeneous smooth volume by the factor $(2\pi R/\lambda)^{1/3}$.

i.e., at r = 10 m, $\frac{\Delta T}{T} = 0.03$ ($\Delta T = 10°K$) or $\frac{\Delta V}{c} = 10^{-2}$ ($\Delta V =$ 3 m/sec). These estimates are arrived at as follows: Consider a jet in which the engines on one wing give rise to an exit velocity difference of 300 m/sec and a temperature difference of 900°K through an area $\pi\, m^2$ (radius 1 meter). When the vortex has spread these gases through an area 316 m^2 (radius 10 meters) the velocity difference is 3.0 m/sec and the temperature difference is 9°K.

The second source of turbulence (i.e., besides exhaust turbulence) is the vortex motion following breakdown. For example, for $\Gamma = 9000$ ft^2/sec (large jet), the velocity in the irrotational outer region is about $V_\varphi = (150\, m^2/sec)/R$; at R = 10 m, $V_\varphi \sim 15$ m/sec. We assume that a fluctuating velocity of 3 m/sec is consistent with this vortex.

In the following estimates of signal power, we assume that the wake fills the beam in these estimates. For an antenna aperture of 3 meters the beam width is about 2.5° at λ = 2 kHz and at a range of 500 m is 25 m broad.

Thus the expression for the received power takes the form

$$P_r = 10^{-8}\, \frac{\cos^2\theta \cos^2\frac{\theta}{2}}{\sin^{(11/3)}\frac{\theta}{2}} \left[\left(\frac{C_{v/C}}{10^{-3}} \right)^2 + 0.13 \left(\frac{C_{T/T}}{10^{-3}} \right)^2 \right]$$

$$\times \left(\frac{\lambda}{0.3} \right)^{1/3} \left(\frac{P_T}{1 \text{ joule}} \right) \frac{(A/10\ m^2)}{(R/500\ m)^2} \quad \text{watts} \qquad (8.7)$$

Atmospheric absorption will determine the maximum usable frequency. For a total path length of 1 km at 1 kHz we expect about 3 db absorption due to water vapor in a 50%

humid atmosphere at 20°C (Harris 1966). At higher frequencies the absorption coefficient increases as f^2.

Little (1969), in considering similar acoustic systems for an atmospheric backscatter sonar, assumed an overall efficiency for the collector-detector-recording system of 4% (-14.5 db). We will also use this value for our reference system thus giving an overall loss including absorption of 17.5 db ($\xi = .02$) at 1 kHz) for a total path length of 1 km.

The received power may be expressed in the form

$$P_r = 2 \times 10^{-10} \frac{\cos^2\theta \cos^2\frac{\theta}{2}}{\sin^{(11/3)}\frac{\theta}{2}} \left[\left(\frac{C_{v/c}}{10^{-3}}\right)^2 + 0.13\left(\frac{C_{T'/T}}{10^{-3}}\right)\right] \frac{P_T}{lj}$$

$$\times \frac{(A/10\ m^2)}{(R/500\ m)^2}\left(\frac{\xi}{0.02}\right) \text{ watts} . \qquad (8.8)$$

Background Noise

It is expected the background noise will limit the sensitivity of an atmospheric sonar system. In Table I we have tabulated noise levels for various typical situations referenced to the standard sound pressure of 2×10^{-4} dynes/cm^2 (10^{-16} w/cm^2/octave at 1 kHz). For our present estimates we will express the noise power in terms of a reference level of 10^{-16}w/cm^2/octave at 1 kHz which would normally be considered close to hearing threshold. The background noise power varies roughly as the band width and inversely as the cube of the frequency ($\Delta f/f^3$). Since the effective collector aperture for coherent systems is $\lambda^2/4\pi$ (if the noise is isotropic), we may express the detected noise power at threshold (10^{-16} w/cm^2/octave) as

TABLE 8.2: TYPICAL NOISE LEVELS

db above $p_o = 2 \times 10^{-4}$ dynes/cm^2

0	Very quiet	~ Threshold of hearing
10		
20	Quiet	Quiet suburban location
30		
40		
50	Average	Ordinary conversation
60		
70	Noisy	Busy traffic
80		
90	Very noisy	Piston engine aircraft cabin
100		
110		
120		Discomfort threshold
130		
140		Threshold of pain

$$P_N = P_{N_t} = 7 \times 10^{-17} \left(\frac{\Delta f}{100}\right)\left(\frac{1000}{f}\right)^5\left(\frac{\xi_N}{0.1}\right) \quad \text{watts} \qquad (8.9)$$

where ξ_N is the transducer efficiency.

Example Calculation: Bistatic forward scatter anode

For a target at 100 meters height and 1 km from source to receiver, $\theta/2 = 0.2$

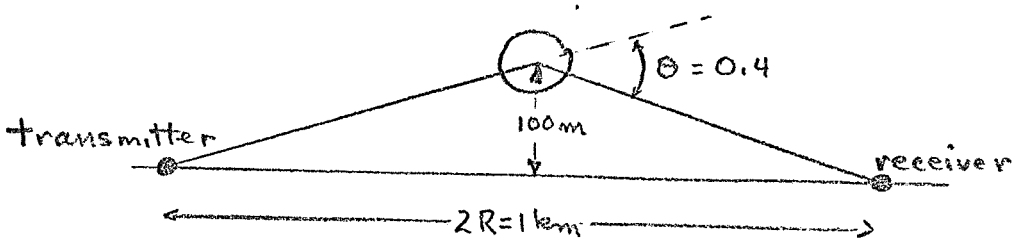

Figure 8.1

and

$$P_r = 2 \times 10^{-10} \cos^2(0.4) \cos^2(0.2)/[\sin(0.2)]^{11/3} \qquad (8.10)$$

$$= 0.6 \times 10^{-7} \text{ watts}$$

For backscatter there is no contribution from the velocity structure. However, under conditions where scattering by thermal irregularities is comparable to the assumed velocity fluctuation ($.13\, C_T^2/T^2 \simeq 10^{-6}$ cm$^{-2/3}$) in our assumed nominal case, the backscatter would be of order 2×10^{-10} watts, i.e., about a factor 300 times smaller than for forward scattering.

The signal to noise ratio (i.e. signal to background) is given by

$$N = \frac{P_r}{P_N} = \frac{3 \times 10^6 \times \dfrac{\cos^2\theta \cos^2\theta/2}{\sin^{(11/3)}\theta/2} \left(\dfrac{C_v/C}{10^{-3}}\right)^2 \left[1 + .13\left(\dfrac{C_T/T}{C_v/C}\right)^2\right]\left(\dfrac{P_T}{1j}\right) \dfrac{(A/10m^2)}{(R/500m)^2} \left(\dfrac{\xi}{.02}\right) \alpha}{\left(\dfrac{\Delta f}{100}\right) \left(\dfrac{1000}{f}\right)^5 \left(\dfrac{\xi_N}{0.1}\right) (P_N/P_{N_t})} \tag{8.11}$$

where α is the absorption loss (referenced to a standard loss of 3 db):

$$\alpha = e^{-0.693 \left[\left(\frac{R}{500m}\right) \left(\frac{f}{1000}\right)^2 - 1\right]} \tag{8.12}$$

Thus, for forward scatter where $\theta << 1$,

$$\frac{S}{N} = \frac{6 \times 10^8}{(P_N/P_{N_t})} \frac{\left(\dfrac{0.2}{\theta}\right)^{11/3} \left(\dfrac{C_v/C}{10^{-3}}\right)^2 \left[1 + .13 \left(\dfrac{C_T/T}{C_v/C}\right)^2\right] \left(\dfrac{P_T}{1j}\right) \left(\dfrac{A}{10m^2}\right) \left(\dfrac{\xi}{.02}\right) \alpha}{(R/500m)^2 \ (\Delta f/100) \ (1000/f)^5 \ (\xi_N/0.1)} . \tag{8.13}$$

Here P_N/P_{N_t} is the ratio of the background noise power to the threshold level. For our reference geometry (R = 500 m, A = 10 m^2, $C_v/C = 10^{-3}$ $cm^{-1/3}$, or $C_T/T = 3 \times 10^{-3}$ $cm^{-1/3}$, $\theta = 0.2$) and at 1 kHz with 10 ms pulses (i.e., $\Delta f \simeq 100$ sec^{-1}) a signal to background noise level of 10 db or better can be expected when the background noise power is less than 10 db. Such a noise level corresponds to a fairly noisy environment (equivalent to busy traffic).

Although specific information concerning vortex turbulence levels and actual airport noise would be required to establish real feasibility in that environment, the sensitivity of this non-optimized forward scatter system appears high enough that further investigation is warranted.

Backscatter Mode

At backscatter and assuming that values of C_T/T of the order 0.003 $cm^{1/3}$ occur in jet aircraft wakes, the signal to background noise at 1 kHz is about 25 db lower than the above

estimates. In order to have S/N = 10, the noise background must be less than 52 db. This is a level characteristic of normal conversation and such a backscatter system may be marginal or even inoperable in an airport environment.

Since side scatter systems ($\theta = 90°$) do not produce detectable signals from velocity fluctuations because of the $\cos^2\theta$ term, the forward scatter technique is strongly favored in moderately noisy environments. Near direct forward scatter is to be avoided in general because of the difficulty of separating the direct pulse from the scattered pulse. In the system considered, the scattered pulse arrives 3 pulse widths (30 ms) behind the direct pulse. However, scattering from solid objects (ground roughness, buildings, etc.) on the ground can be expected to give rise to strongly competing delayed echoes unless the antennas are highly selective. At backscatter these echoes could be suppressed to some extent by utilizing the fact that the vortex signal will be doppler shifted due to the convection velocities in the vortex. A 7 meter/second velocity results in a frequency shift of about 50 Hz. In order to utilize this effect pulses longer than 20 ms (range resolution of 50 feet) must be utilized. By using a 100 ms pulse and a band width of 10 Hz it would probably be possible to reject moderately strong signals from stationary obstacles and ground return. Although the backscatter power is down by 25 db from the forward scatter case considered ($\theta = 0.2$) the narrower band width allows 10 db of this reduction to be recovered (yielding an S/N of 10 in a background noise of 62 db).

In general there would seem to be little problem in obtaining a detectable return in a quiet environment when the antennas and electronics used can suppress clutter echoes. We

need measured data for the real airport environment and better estimates of the scattering cross section of trailing vortices and of the background clutter problem to reach realistic conclusions for an operational acoustic vortex detection system. Also good estimates for achievable frequency characteristics and pulse shapes (especially the trailing edge) of high power audio transmitters are required to determine the feasibility of detecting weak signals shortly after transmission of a strong pulse.

Optimization of the characteristics of the system can be expected to improve somewhat the signal/noise estimates. In the example chosen we consider a baseline for the forward scatter mode of 1 km. Reduction of this distance will allow the use of a higher frequency resulting in a strong reductionin background noise. In the backscatter mode operation at shorter ranges and higher frequencies results in strong improvement in signal to noise since the S/N effectively varies as $R^{-9/2}$ when the product f^2R is held constant in order to maintain constant atmospheric absorption. The gain due to reducing the range is not so marked in the forward scatter mode since the scattering angle increases with decreasing range.

Having completed this preliminary analysis we are now carrying out a more detailed study of atmospheric sonar systems for aircraft wake detection, attempting to improve and limit the values of the various input parameters and to identify optimum configurations.

IX. AIRCRAFT WAKE VORTICES: Fluid Dynamics

SUMMARY

An analysis is in progress to develop a theory for the structure and decay of turbulent line vortices. A portion of this analysis is an extension of the theory of Hoffman and Joubert to allow treatment of the core region and to account for the axial decay of the vortex. The initial approach is to assume a completely turbulent vortex, introduce a Prandtl mixing length hypothesis, consider turbulent transport only in the radial direction but allow convection both radially and axially (and of course tangentially). Of primary interest is the axial decay of the vortex and the phenomena of vortex breakdown. The analysis has been formulated and effort is currently in progress to obtain both approximate and "exact" solutions. The equations for similarity solutions have been formulated for the full set of equations. The present analysis is proceeding in two directions:

1) to solve for the self similar solutions and

2) to divide the vortex structure into three regions: an inner core, an intermediate self preserving region and an outer region. In the intermediate region the turbulent stresses are high, and radial and axial convection of momentum can be neglected. This assumption leads to the self preserving logarithmic growth of the circulation with radius predicted theoretically and confirmed experimentally by Hoffman and Joubert. In the inner region the axial velocities can be shown to be comparable to the tangential velocities and convection of momentum cannot be ignored. That the axial and tangential velocities are indeed of comparable magnitude in aircraft wake vortices is

apparently evident in some of the smoke visualization pictures taken recently by NASA at NASA-MSFC. In order to compare with the theoretical development it would be highly desirable to obtain quantitative reduction of these photographs in terms of rotation velocities and axial velocities as a function of radius and distance downstream of the aircraft. If further flights should be scheduled it is suggested that photograph coverage be obtained with a clock and with distance scales in the field of view. Also the ambient wind velocity should be measured, and the aircraft lift and drag needs to be known.

It would also be desirable to obtain motion picture coverage from two different stations so that stereo reduction is possible. This is of particular importance at vortex breakdown where there has been some indication of negative rotations.

Summary of present theory

The trailing vortex system of an aircraft results from the development of lift about the wing. At large distances behind the aircraft, the lift-induced circulation tends to concentrate in two "tip" vortex lines of opposite circulation. This concentration is due to upwash around the tip of the wings and the resultant rolling up of the vortex sheet shed from the trailing edge of the wing. Tangential velocities in these vortices depend to some extent upon the details of their formation, and generally increase with increasing lift or aircraft weight. Several accidents in small aircraft near airports have been ascribed to the vortex wakes of large jets which passed through shortly before. The vortex system of "jumbo" jets is expected to involve higher velocities and to persist for longer time before ultimately dissipating.

If there were no local winds, one would expect the vortex lines to move downward, under their mutual influence, and outward, under the influences of their images below the ground plane, as shown below:

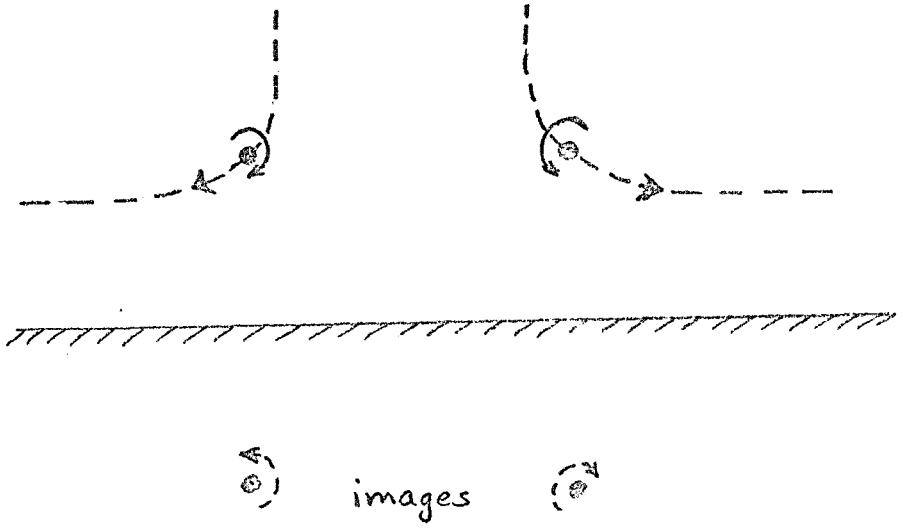

Figure 9.1

Attempts to correlate measured vortex motions at airports with this simple picture have been unsuccessful. Apparently, the influence of local winds, including random gusts, upon vortex line motion, is very strong. One therefore expects the prediction of vortex position to be difficult in the absence of detailed information on the local wind and its gust structure as a function of time.

Our quantitive understanding of the flow within the kind of vortex produced by large aircraft is not good, although a qualitative picture has emerged as the result of several investigations. The flow in these vortex systems is probable turbulent. Prediction of the flow structure from inviscid or laminar concepts agrees neither with wind tunnel nor field measurements. A study of turbulent line vortex structure by Hoffman and Joubert incicates that certain ideas from boundary layer theory can be applied to these flows. Applying this line of reasoning to a rotating flow in which angular momentum is conserved, they deduced that there should be a region of the flow in which the circulation varies as log r. Inside of this region the fluid should rotate as a rigid body ($v \sim r$), and outside of it the circulation should approach a constant value. The variation of the circulation and tangential velocity should then look as follows:

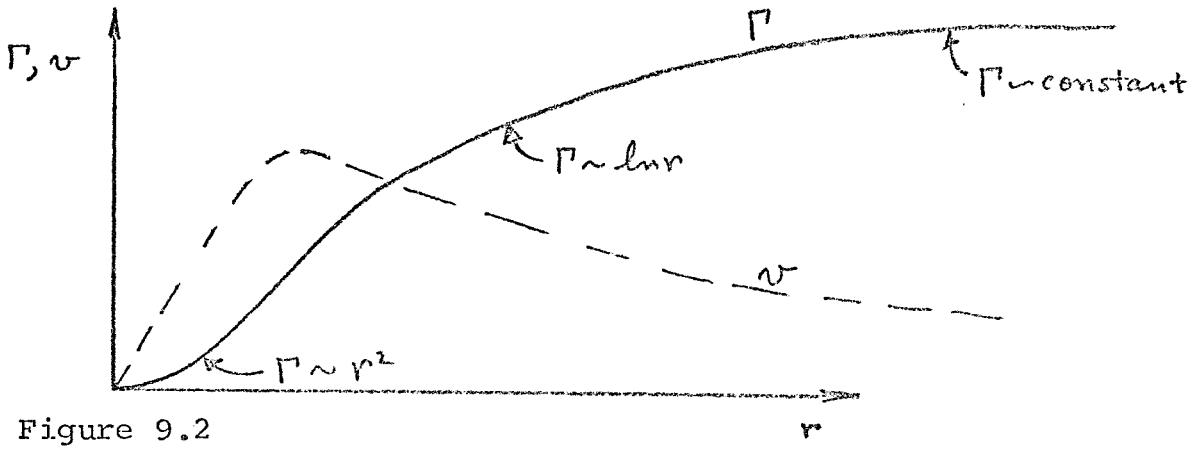

Figure 9.2

Dimensional analysis leads to the conclusion that

$$\frac{\Gamma}{\Gamma_\infty} = f\left(\frac{vz}{\Gamma_o} , r/z , \frac{uz}{\nu} \right)$$

where Γ_∞ is the free-stream circulation, u the free stream velocity, z the downstream distance (normal to the plane of rotation, or along the vortex line), and ν the kinematic viscosity. The principle of Reynolds number invariance in a fully turbulent flow implies that in a fully turbulent vortex the dependence on U_z/ν vanishes. Experiments in a wind tunnel showed that there was indeed a logarithmic region of the circulation profile for vortices with $U_z/\Gamma_o > 150$, and that there appeared to be a "universal" profile for the core region analogous to the wall region of a turbulent boundary layer. Unlike the wall, however, fluctuating velocities in the inner region need not be low. Not enough is known about the circulation at large r to establish a "defect" law for the outer regions of the vortex. Such a law would be analogous to the "law of the wake" for a boundary layer.

A field study of turbulent vortices performed by McCormick, Trayler and Sherrieb indicates that vortices generated immediately behind the wings of small aircraft (Army O-1 and Piper Cherokee) follow the laminar behaviour, but undergo a transition to the logarithmic form at some downstream distance. They hypothesize that this change may be associated with vortex breakdown rather than transition. "Turbulent" vortex structure is associated with wing midchord Reynolds number $\geq 3 \times 10^6$. Their data suggests that the circulation at the maximum tangential velocity varies linearly with C_L. The combination of their wind-tunnel and field data offers a set of semi-empirical relationships which can be used to estimate the tangential velocity profile in a vortex system as a function of time after the passage of the aircraft.

Since their data show the the core circulation to be nearly constant, $V_{max} \sim t^{-\frac{1}{2}}$ and $r(V_{max}) \sim t^{\frac{1}{2}}$.

For a typical "jumbo" jet they predict values for the tangential velocity of over 100 ft/sec one minute after passage and 55ft/sec five minutes after passage. Velocities of over 40 ft/sec should persist over several feet from the vortex core (see Figure 1).

In some of the model data, negative rotations were measured near the center of the vortex system at large times. It is by no means clear how these are produced, although three-dimensional effects are probably involved. However, they are in the direction of the logarithmic distribution, which predicts low velocities in the vortex core.

In interpreting a scattered signal, axial velocities in the vortex system, as well as tangential, must be accounted for. Because the core tangential velocities vary with z , a pressure gradient is induced which tends to push fluid along the core in the direction of the aircraft wing. The acceleration of this fluid is an induced drag on the wing. Batchelor has estimated the axial velocities in a vortex core of the exponential laminar form; he concludes that in some cases, particularly if $v > u$, the axial velocity is of the same order as V_{max}. At large downstream distances, he predicts that $(u - V_{max}) \sim z^{-1} \log z$.
We do not know of any experimental studies of axial velocities in trailing vortices, or of any attempts to predict axial velocities when the flow is fully turbulent.

Since the transition to the logarithmic circulation distribution may be associated with vortex breakdown, and is certainly associated with turbulent flow, the prospect of large fluctuating axial, radial and tangential velocities exists. These would add to the complexities of a back-scattered signal. We know of no studies of velocity fluctuations in vortex flows; some analogies with other turbulent flows (local isotropy of small eddies, ratio of large-eddy fluctuation to mean-flow velocities, and ratio of outer scale to flow dimensions) may be possible. Scrutiny of some smoke trail photographs of vortex breakdown suggests that the flow pattern may be more complicated than mean velocity studies indicate.

The surface wind structure associated with the vortex is of interest, since, if vortex-induced surface velocities are comparable to or larger than velocity fluctuations due to gusts in the local wind, they might be used to detect the presence of the vortex. The estimates of McCormick et al. lead one to expect surface winds of the order of 10ft/sec. for large aircraft. It therefore appears difficult to detect vortices on a gusty day by wind velocity measurement near the surface; even on still days, the local wind will be affected by aircraft thrust and fuselage drag and detection may be difficult.

The Radius of the Core before Diffusion

The kinetic energy per unit length contained within a radius r of a vortex having a core radius a is given by

$$\epsilon = \pi \int_0^r \rho V^2 r dr$$

$$= \frac{\Gamma^2 \rho}{4\pi} \left[\tfrac{1}{4} + \ell n r/a \right] \qquad (9.2)$$

Here $V = \Gamma r/2\pi a^2$ for $r < a$ and $V = \Gamma/2\pi r$ for $r > a$. Equation gives the energy for an isolated vortex. For a vortex pair, separated by a distance b, the energy is, approximately, (Spreiter and Sacks (1960)).

$$\epsilon_i \approx \frac{\Gamma^2 \rho}{2\pi} \left[\tfrac{1}{4} + \ell n \left(\frac{b-a}{a} \right) \right] \qquad (9.3)$$

Actually this is an underestimate since it does not take into account the forward velocity of the air in the case of the vortex. This energy gain by the atmosphere results in a loss of energy by the aircraft. The energy input into the air per unit length is the induced drag. Equating the wake kinetic energy to this drag yields (Spreiter and Sacks (1960)) for an elliptically loaded wing

$$\frac{a}{b} = \left(1 + \exp \left[\frac{\pi^2 - 1}{4} \right] \right)^{-1} = 0.0985 \qquad (9.4)$$

Thus, for a 100 foot vortex separation, the initial core diameter is expected to be about 20 feet.

The smoke entrainment measurements by NASA show considerable structure within this calculated core. In Figure a photograph of the smoke entrained into the vortex from a tower mounted smoke bomb is shown. The central part of the core is made visible by smoke entrained at one station and then sucked along the vortex center by the axial pressure gradient. In the photographs shown the vortex height above the ground (b/2) is approximately equal to the tower height, and the visible core radius is about 2.5% of this height, i.e. about 0.0125 b and very much smaller than the calculated core radius. Although there is some question as to the relevance of the details of the core structure to the problem of predicting aircraft rolling moment (Section) it is clear that simplified inviscid models that do not account for axial motion do not provide a complete description of the vortex structure. More laboratory and field measurements in addition to a three dimensional theory are needed.

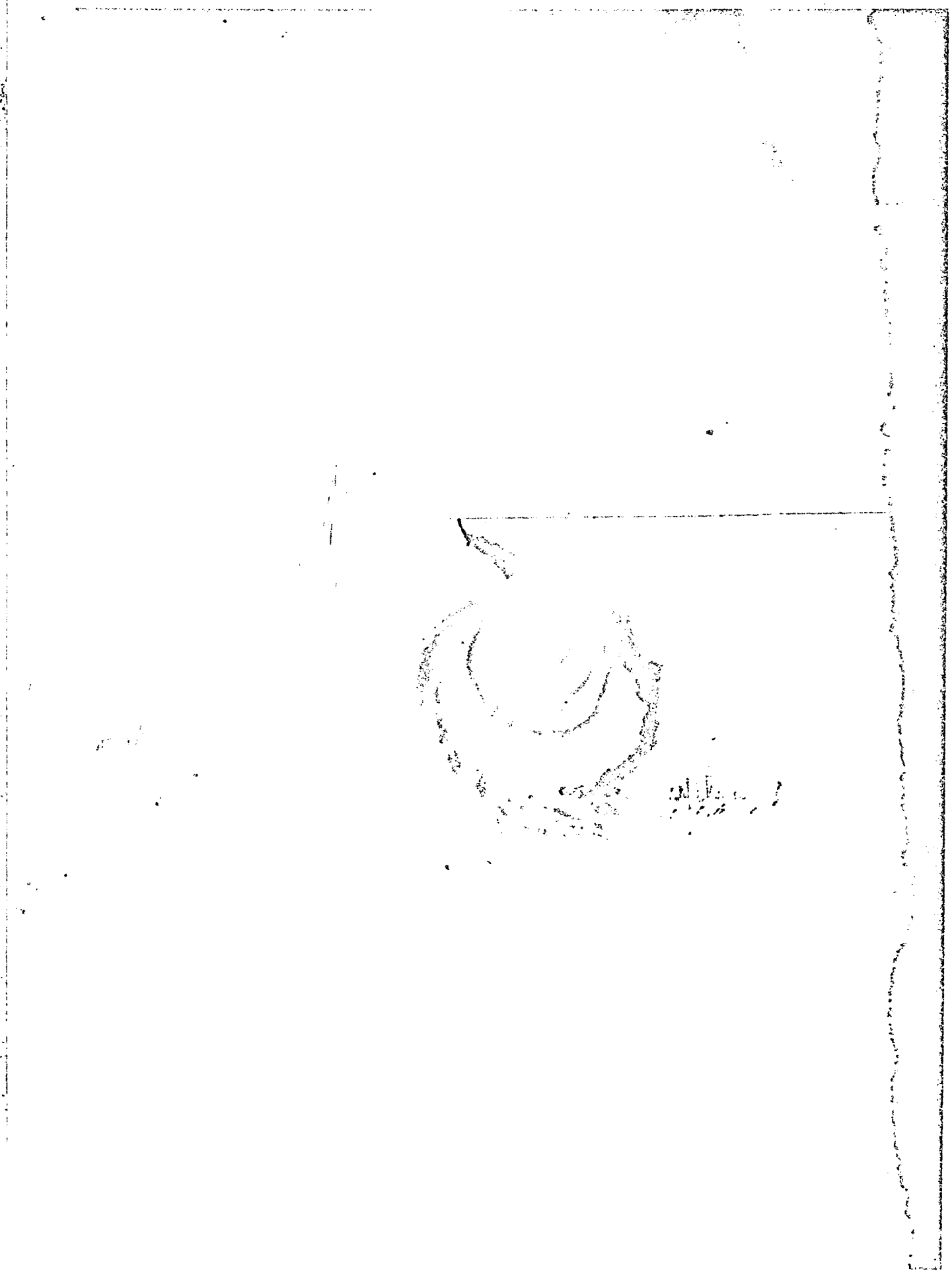

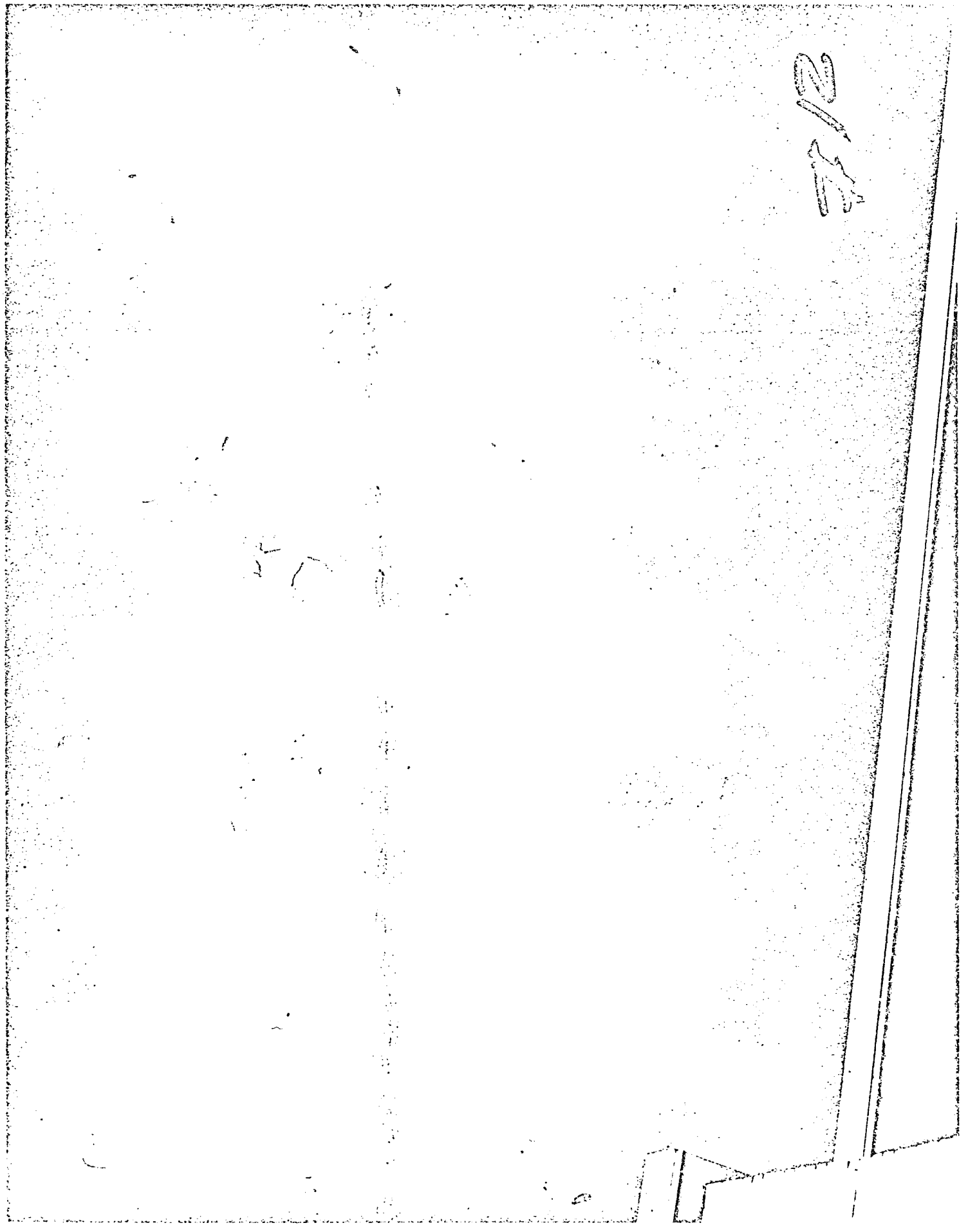

Laminar diffusion and decay of a cylindrical line vortex

The decay of a cylindrical line vortex is governed by the equations:

$$\frac{\partial v}{\partial t} = \frac{1}{r^2}\frac{\partial}{\partial r}\left(r^2\frac{\tau}{\rho}\right) = \frac{\nu}{r^2}\frac{\partial}{\partial r}\left(r^3\frac{\partial}{\partial r}\left(\frac{V}{r}\right)\right) \tag{9.5}$$

where ν is the kinematic viscosity. These equations admit a similarity solution of the form

$$V(r,t) = \frac{\Gamma}{2\pi r}\left[1 - \exp(-r^2/4\nu t)\right] \tag{9.6}$$

where Γ is the total circulation at large radii. The core radius in this case grows as

$$\begin{aligned} a &\sim \sqrt{2\nu t} \\ &= 0.6\sqrt{t(\text{sec})} \text{ cm in sea level air} \\ &= 0.2\sqrt{t(\text{sec})} \text{ cm in water} \end{aligned} \tag{9.7}$$

Thus, except in small scale simulation experiments, the laminar diffusion growth is very slow, and can be neglected for practical purposes.

The characteristic times for a trailing vortex wake to develop instabilities due to the mutual interaction of the two vortices is of the order of $\tau = 2\pi b^2/\Gamma$ where b is the vortex separation (the downward velocity $v = \Gamma/2\pi b$) and experiment times or measurement times should be several times this value. Thus the core radius (a*) at the time τ is given by

$$(a^*)_{lam} = b\sqrt{4\pi\,\nu/\Gamma} \tag{9.8}$$

We can define a characteristic Reynolds number according to

$$Re = \Gamma/4\pi\nu \tag{9.9}$$

and write

$$(a^*)_{laminar} = b/\sqrt{Re} \tag{9.10}$$

Turbulent diffusion and decay of a line vortex

In most cases of practical interest for aircraft wakes the laminar or molecular diffusivity is expected to be of minor importance. The characteristic distances associated with molecular diffusion effects can be estimated as the simple diffusion distance in a laminar flow ($\ell_m \sim \sqrt{4\nu t}$) or as the inner scale(ℓ_1) in a fully turbulent flow. This latter distance is to order of magnitude related to the energy dissipation rate according to the expression

$$\ell_1 \sim \nu^3/E^{\frac{1}{4}} \tag{9.11}$$

The rate at which energy is being fed into the turbulent motion

is of order.

$$\epsilon \sim \alpha V^3/\ell_o \tag{9.12}$$

where V_o and ℓ_o are the macroscopic velocities and dimensions characteristic of the turbulent region and α is a numerical constant (α is essentially half the fractional energy loss from an eddy in the characteristic eddy cycle time ℓ_o/V). Thus

$$\ell_1 \sim \left(\frac{\nu^3 \ell_o}{\alpha V^3}\right)^{\frac{1}{4}} \tag{9.13}$$

and the ratio ℓ_1/ℓ_o is given by

$$\frac{\ell_1}{\ell_o} = \left(\frac{\nu^3}{\alpha \ell_o{}^3 V^3}\right)^{\frac{1}{4}} = \frac{1}{\alpha^{\frac{1}{4}}(Re)^{3/4}} \tag{9.14}$$

where Re is the Reynolds number of the flow ($Re = V\ell_o/\nu$) . Taking V as the tangential velocity at the edge of the core and ℓ_o equal to the core radius (a), we have

$$Re = \frac{1}{2\pi} \frac{\Gamma_c}{\nu} \tag{9.15}$$

where Γ_c is the core circulation. For air ($\nu = 0.15 cm^2/sec$) and a core circulation of the order of one half the total circulation of a large jet vortex ($\Gamma_c \sim \frac{1}{2}\Gamma_\infty \sim 4.5 \times 10^6 cm^2/sec$) we obtain

$$Re \sim 0.7 \times 10^6 \tag{9.16}$$

and

$$\frac{\ell_1}{(a)_{turb}} = 4 \times 10^{-5}/\alpha^{\frac{1}{4}} \tag{9.17}$$

For comparison the laminar diffusion distance in a time (a/V_c) is given by

$$\left(\frac{\ell_m}{(a)}\right)_{turb} = 2\sqrt{2\pi\nu/\Gamma_c} = 2/\sqrt{Re} \sim 1/430 \tag{9.18}$$

and the ratio of the inner scale to this laminar diffusion distance is

$$\frac{\ell_1}{\ell_m} \sim \tfrac{1}{2}(\alpha Re)^{\frac{1}{4}} \tag{9.19}$$

The value of the factor α in typical turbulent shear flows (boundary layer, jets, wakes) is of the order of 0.02 so that in the regions of the vortex that are turbulent:

$$\left(\frac{\ell_1}{a}\right)_{turb} \approx 2.7/Re^{3/4} \sim 10^{-4} \tag{9.20}$$

and

$$\frac{\ell_1}{\ell_m} \approx 0.043 \tag{9.21}$$

Thus to a good approximation the inner scale is very much less than the expected outer scale and an infinite Reynolds number model is applicable.

Mathematical Formulation for Turbulent Vortices

In this study we are attempting to extend the analysis of turbulent line vortices beyond the zero radial velocity model considered by Hoffman and Joubert and to include the decay of the vortex with down stream distance. We assume a fully turbulent vortex in an incompressible fluid, and eliminate all laminar viscous terms. In the analysis at its present state the turbulent Reynolds stresses have only been retained in the tangential momentum equation and inviscid forms are used for the radial and axial equations. We are presently attempting to obtain solutions of these equations using the same assumptions concerning the tangential Reynolds stress as did Hoffman and Joubert (that is a Prandtl mixing length model plus the assumption that the eddy diffusivity depends only on the local tangential stress and on the radius). The resulting formalism includes the self preserving region studied by Hoffman and Joubert in the region of high turbulent stress, but also allows for radial and axial convection. Present analysis is directed towards evaluating similarity solutions to these equations. In the remainder of this section we describe the mathematical formalism.

At steady state, the tangential momentum equation may be expressed in the form (assuming axial symmetry).

$$\rho \left[U \frac{2V}{2r} \quad \frac{UV}{r} + W \frac{\partial V}{\partial z} \right] = \frac{1}{r^2} \frac{\partial}{\partial r}(r^2 \tau_{r\varphi}) + \frac{\partial}{\partial z}(\tau_{\varphi z}) \tag{9.22}$$

where U is the radial velocity, V the tangential velocity and W the axial velocity. In terms of the viscosity μ the laminar stresses are

$$\begin{aligned} \tau_{r\varphi}/\rho &= (\mu/\rho) \left[r \frac{\partial}{\partial r} (V/r) \right] \\ \tau_{\varphi z}/\rho &= (\mu/\rho) \frac{\partial V}{\partial z} \end{aligned} \tag{9.23}$$

The continuity equation for incompressible flow requires

$$\frac{1}{r}\frac{\partial}{\partial r}(rU) + \frac{\partial W}{\partial z} = 0 \tag{9.24}$$

Rewriting the momentum equation:

$$\frac{U}{r}\frac{\partial}{\partial r}(rV) + W\frac{\partial V}{\partial z} = \frac{1}{r^2}\frac{\partial}{\partial r}\left(r^2\frac{\tau_{r\varphi}}{\rho}\right) + \frac{\partial}{\partial z}(\tau_{\varphi z}/\rho). \tag{9.25}$$

We neglect the transport term due to axial gradients on the basis that these gradients are small compared to the radial ones:

$$\frac{U}{r}\frac{\partial}{\partial r}(rV) + W\frac{\partial V}{\partial z} = \frac{1}{r^2}\frac{\partial}{\partial r}\left(r^2\frac{\tau_{r\varphi}}{\rho}\right) \tag{9.26}$$

The radial and axial momentum equations are (neglecting the transport terms)

$$\begin{aligned} U\frac{\partial W}{\partial r} + W\frac{\partial W}{\partial z} + \frac{1}{\rho}\frac{\partial p}{\partial z} &= 0 \\ U\frac{\partial U}{\partial r} - V^2/r + W\frac{\partial U}{\partial z} + \frac{1}{\rho}\frac{\partial p}{\partial r} &= 0 \end{aligned} \tag{9.27}$$

Since the axial velocity W also exhibits strong radial gradients we should include a transport term (turbulent) in the axial momentum equation. Although recognizing that this term may be significant we will ignore this complication in the present analysis in order to simplify the computation.

We expect radial velocities U much less than the tangential velocities. Axial velocities (W) are much greater than the radial ones since

$$\left|\frac{\partial U}{\partial r}\right| \approx \left|\frac{\partial W}{\partial z}\right| . \tag{9.28}$$

Experimentally axial velocities in the core may be comparable to the peak tangential velocities. Thus $U \frac{\partial U}{\partial r}$ and $W \frac{\partial U}{\partial z}$ may both be neglected compared to V^2/r:

$$-\frac{V^2}{r} + \frac{1}{\rho}\frac{\partial p}{\partial r} \approx 0 \tag{9.29}$$

On the centerline of the vortex ($u = o$, $\rho = P_{C_L}$):

$$W \frac{\partial W}{\partial z} + \frac{1}{\rho}\frac{\partial P_{C_L}}{\partial z} = 0 \tag{9.30}$$

or

$$P_{C_L} + \rho W_{C_L}^2/2 = \text{constant} = P_o . \tag{9.31}$$

To correlate the magnitude of the axial and tangential velocities, we approximate V by the relations

$$\begin{aligned} V &\sim V_o \; r/r_o \quad \text{for } r < r_o \\ &\sim V_o \; r_o/r \quad \text{for } r > r_o \end{aligned} \tag{9.32}$$

and integrate the radial equation to find to order of magnitude:

$$P_o - P_{C_L} \sim \rho V_o^2 \tag{9.33}$$

so that

$$W_{C_L} \sim \sqrt{2} V_o \tag{9.34}$$

Summarizing these results we have

$$\frac{U}{r}\frac{\partial}{\partial r}(rV) + W\frac{\partial V}{\partial z} = \frac{1}{r^2}\frac{\partial}{\partial r}(r^2 \tau_{r\varphi}/\rho)$$

$$V^2/r \approx \frac{1}{\rho}\frac{\partial p}{\partial r} \qquad (9.35)$$

$$U\frac{\partial W}{\partial r} + W\frac{\partial W}{\partial z} + \frac{1}{\rho}\frac{\partial p}{\partial z} = 0$$

and

$$\frac{1}{r}\frac{\partial}{\partial r}(rU) + \frac{\partial W}{\partial z} = 0.$$

The zero radial convection model of Hoffman and Joubert

In the analysis of Hoffman and Joubert it is assumed that there is a self preserving region where the turbulent stress is high and is much greater that required by the radial and axial convection of angular momentum (the LHS of the tangential momentum equation) - i.e. that there is a region in which the eddy viscosity is much greater than is required to accelerate the flow to the local tangential velocity as it drifts inwards radially.

Under these conditions

$$\frac{\partial}{\partial r}(r^2 \tau_{r\varphi}/\rho) \approx 0 \qquad (9.36)$$

and thus

$$\tau_{r\varphi}/\rho \approx A/r^2 \qquad (9.37)$$

where A is a constant. This is equivalent to assuming that there is a core region which is much smaller than the region of strong radial transport of tangential momentum and that the fluid drifts towards the axis at a much smaller rate than the rate at which momentum can diffuse radially.

We assume the existence of an inner dimension r_o and an outer dimension R_o which limit this region of high diffusive transport of momentum. Again following Hoffman and Joubert we assume that a Prandtl mixing length hypothesis may be applied to this region ($r_o << r << R_o$).

Assuming that when a fluid element is displaced by random convection from a radius r_1 to a radius r_2 it carries with it the mean tangential momentum (ρv) at r_1, the value of the tangential component of this element at the radius r_2 is $(\rho v)_1 r_1/r_2$ and exceeds the local tangential momentum at r_2 by an amount

$$\frac{(\rho v r)_1}{r_2} - \frac{(\rho v r)_2}{r_2} \approx - \frac{\Delta r}{r_2} \frac{d}{dr} (\rho V r) \tag{9.38}$$

where Δr is the radial displacement $(r_2 - r_1)$.

Assuming that the fluctuating component of the tangential velocity $\sqrt{\overline{v'^2}}$ is due to fluid displacement from an average mixing distance ℓ (i.e. that the fluid retains its memory of its momentum over displacements up to a length ℓ) we have

$$- \rho \sqrt{\overline{v'^2}} \approx - \frac{\ell}{r} \frac{d}{dr} (\rho V r). \tag{9.39}$$

The Reynolds stress is given by

$$\tau = - \rho \overline{u'v'} = - \beta \sqrt{\overline{u'^2}} \sqrt{\overline{v'^2}} \tag{9.40}$$

where β is defined by the statement

$$\beta \equiv \overline{u'v'} / \sqrt{\overline{u'^2}} \sqrt{\overline{v'^2}} \quad . \tag{9.41}$$

Thus

$$\tau/\rho = -\beta \ell \sqrt{\overline{u'^2}}\ \frac{1}{r}\ \frac{d}{dr}\ (rV)$$

$$= \nu_T\ \xi \qquad (9.42)$$

where ξ is the vorticity $\left(\xi = \frac{1}{r}\frac{d}{dr}(rV)\right)$ and ν_T the kinematic eddy viscosity.

Hoffman and Joubert show that if it is assumed that the eddy viscosity is required to be a function only of the local shear stress and the radius then dimensional arguments for the equation

$$\tau/\rho = f(\tau/\tau, r)\xi \qquad (9.43)$$

require that

$$\tau/\rho = \mathcal{K}\sqrt{\tau/\rho}\ r\xi \qquad (9.44)$$

where $\mathcal{K}$ is a number, and thus

$$\nu_T = \mathcal{K}\sqrt{\tau/\rho}\ r$$

and

$$\tau/\rho = \mathcal{K}^2 r^2 \xi^2 . \qquad (9.45)$$

In the self preserving region ($r_o << r << R_o$)

$$\tau/\rho \approx A/r^2 \qquad (9.46)$$

so that the eddy viscosity is independent of radius in this region:

$$\nu_T = \mathcal{K}/\overline{A} \qquad (9.47)$$

Thus, substituting for the vorticity,

$$\frac{A}{r^2} = \frac{\mathcal{K}\sqrt{A}}{r} \frac{d}{dr}(rV) \tag{9.48}$$

we find that the circulation ($\Gamma = 2\pi rV$) has the form

$$\Gamma = \frac{2\pi\sqrt{A}}{\mathcal{K}} \ell n\,(r/R_1) \tag{9.49}$$

and the tangential velocity the form

$$V = \frac{\sqrt{A}}{\mathcal{K}R_1} \frac{R_1}{r} \ell n(r/R_1). \tag{9.50}$$

Here R_1 is a constant.

At very large radii ($r \geq R_o$) these expressions should fail as the circulation approaches the inviscid value (proportional to the aircraft lift). Also at very small radii ($r \leq r_o$) they also fail as the inward convection velocities become large. Note that this latter effect is associated with the value of the induced aircraft drag since the drag is manifested as forward momentum in the vortex ($2\pi\int_o^\infty \rho W r dr$) and thus depends on the value of V_{max} (since $W(r=o) \sim \sqrt{2}\, V_{max}$) and on the radius of the vortex core.

In the non self preserving region we have the equations of motion

$$(1) \qquad V^2/r = \frac{1}{\rho}\frac{\partial p}{\partial r} \tag{9.51}$$

$$(2) \qquad U\frac{\partial W}{\partial r} + W\frac{\partial W}{\partial z} + \frac{1}{\rho}\frac{\partial p}{\partial z} = 0 \tag{9.52}$$

$$(3) \qquad \frac{1}{r}\frac{\partial}{\partial r}(rU) + \frac{\partial W}{\partial z} = 0 \tag{9.53}$$

and (9.54)

$$(4) \quad \frac{U}{r}\frac{\partial}{\partial r}(rV) + W\frac{\partial V}{\partial z} = \frac{\mathcal{K}^2}{r^2}\frac{\partial}{\partial r}\, r^2 \left[\frac{\partial}{\partial r}(rV)\right]^2$$

Conservation relations

Integration of Eq. (2) (multiplied by r) with respect to radius yields the expression

$$\int_0^\infty rU\frac{\partial W}{\partial r}\,dr + \frac{d}{dz}\int_0^\infty (p/\rho + W^2/2)\, rdr = 0 \tag{9.55}$$

or, by parts,

$$\int_0^\infty rU\frac{\partial W}{\partial r}\,dr = WrU\Big|_0^\infty - \int_0^\infty W\frac{\partial}{\partial r}(rU)\,dr \tag{9.56}$$

From (3) we then obtain:

$$\int_0^\infty rU\frac{\partial W}{\partial r}\,dr = \int_0^\infty W\frac{\partial W}{\partial z}\,rdr = \frac{d}{dz}\int_0^\infty \frac{W^2}{2}\,rdr. \tag{9.57}$$

Thus we have

$$\frac{d}{dz}\left\{\int_0^\infty \left(\frac{P}{\rho} + W^2\right) rdr\right\} = 0 \tag{9.58}$$

or

$$\int_0^\infty (P/\rho + W^2)\, rdr = D = \text{constant} \tag{9.59}$$

where D is the forward momentum of the vortex (i.e. one half the aircraft drag).

— The pressure drop to the center of the vortex is (from (1))

$$\rho \int_0^\infty V^2/r \, dr = P_\infty - P(o). \tag{9.60}$$

From (2) at r = 0 (since U(o) = 0)

$$\frac{d}{dz}\left(\frac{P(o)}{\rho} + \frac{W^2(o)}{2}\right) = 0 \tag{9.61}$$

or

$$P(o) + \rho \frac{W^2(o)}{2} = P_\infty = \text{constant} \tag{9.62}$$

Thus the centerline axial velocity W(o) is related to the tangential velocity distribution according to

$$W^2(o,z) = 2\int_0^\infty V^2(r,z) \frac{dr}{r} \quad . \tag{9.63}$$

Instability of a Line Vortex Moving Across a Horizontal Surface

As the pair of trailing vortices approach the ground plane the influence of the ground surface (in the inviscid approximation) may be interpreted in terms of image vortices.

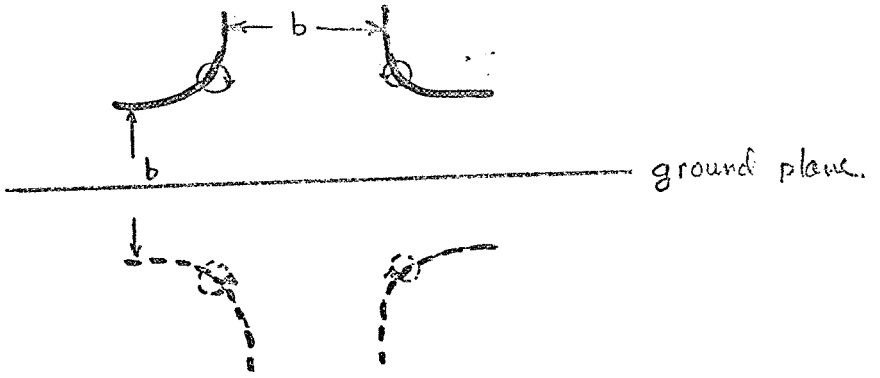

Figure 9.3

In terms of the circulation Γ of the original pair the initial downward velocity is

$$v_o = \Gamma/2\pi b \qquad (9.76)$$

where b is the initial horizontal separation (slightly less than the wing span). Eventually the vortices stabilize at a height b/2 and move horizontally at the initial speed

Crow ( )has examined the stability of a pair of free line vortices moving under their mutual influence. He finds two long wavelength unstable modes, one symmetric about the vertical plane through the aircraft track and the other anti-symmetric. The symmetric mode has the highest growth rate and appears to be the one observed in flight. The instability results in a growing displacement in planes canted roughly 45° to the vertical.

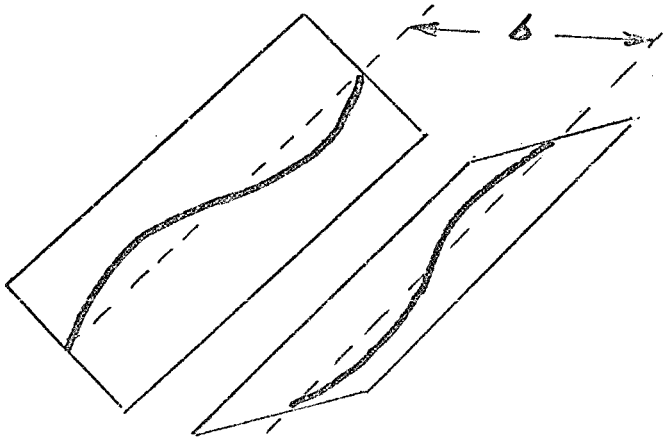

Figure 9.4 Symmetric Instability

The e-folding time for this mode is roughly the time for the vortices to move downward a distance b. In other words, the instability is actually very strong although it is somewhat difficult to observe because of the usual low translational velocity of the vortices.

The wavelength of maximum growth rate is roughly given by

$$\frac{2\pi}{\lambda} b \approx 1 \tag{9.77}$$

or

$$\lambda \sim 6b \tag{9.78}$$

Substituting appropriate expressions for the circulation ($\Gamma \sim W/\rho v b$) we may express the growth time in the form

$$\begin{aligned} \tau &\sim 2\pi b^2/\Gamma \\ &\sim 2\pi\rho V b^3/W \end{aligned} \tag{9.79}$$

where ρ is the ambient density and W the aircraft lift (equals weight in level flight).

Jet aircraft tend to operate at more or less constant values of ρV (of the order of 7 gm/cm^2 - sec) so that the growth time is not sensitive to flight altitude. Since the value of b^3/W tends to be much smaller for jet aircraft than for piston engine aircraft, the growth time is expected to be smaller for jets than for propeller driven aircraft.

Photographs of contrails of jet aircraft at altitude show that the instability develops until the two vortices touch. At this time the wake breaks up into a series of vortex rings which eventually dissipate by diffusion. The breakup is normally only apparent when the atmosphere is locally humid so that the water-

droplets evaporate only slowly and when there is locally only little wind shear. In the presence of significant wind shear the instability is not apparent, the primary visible effect being a simple spreading of the contrail.

When the aircraft is close to the ground the instability may not have time to develop before the ground images take over and the two vortices separate laterally. The time required (and the distance travelled before the instability develops to large amplitude) may be a few e-folding times in quiet air, so that the vortex pair may be able to travel several times the separation distance before breaking up. Thus close to the ground the vortices may be able to negotiate the turn to horizontal motion without breaking up. In this case each vortex primarily sees only its own image. If the effects of diffusion and viscous interaction with the ground do not remove the instability (the turbulent diffusive interaction time is expected to be of the same order as the instability growth time so that only a better theory or an experiment can decide which dominates) the symmetric instability is still permitted. The symmetric mode is the only one which leaves the normal component of the velocity at the ground plane equal to zero, as required by the boundary conditions. Thus we would anticipate the possibility of breakup of the vortex due to this instability within a few times the distance b from the aircraft track (i.e. within a few wing spans).

Even if the instability can grow in the presence of diffusion ring vortices are not expected but, as a section of the vortex dips down toward the ground, the dissipation rate will increase and will tend to destroy the high velocities in the vortex core. Since the pressure in the core will thus rise, creating large axial pressure gradients, this in itself may tend to "blow up" the vortex at points well removed from the ground contact point.

Since the instability amplifies rapidly in the presence of wind shear gradients of appropriate wavelength it may be possible to artificially create local distrubances (with use of ground airjets and ground obstacles) to provide large amplitude perturbations that will enhance the rate of breakup of the vortex. At least it may be possible to ensure aerodynamic isolation of adjacent runways by such techniques.

Both laboratory and field experiments are appropriate. In the field it would be desirable to determine if the mutual instability mechanism is actually operative close to the ground. For this purpose it would be necessary to follow the vortex both in its motion across the ground and at several different axial stations. Laterally a distance of a few (3-4) times the wing span b should be diagnosed and longitudinally at least a distance $2\pi b \sim (6\text{-}8)b$. Multiple towers with smoke bombs are appropriate. A square grid of 16 towers (height $\sim b/2$), 4 towers on a side would probably be sufficient. Ground pressure and velocity measurements would be desirable but should have somewhat finer grid spacing. A laser scanning system should be attempted and needs to be a truly 3-D measurement in order to guarantee detection after breakup.

Turbulent decay time

The characteristic energy dissipation rate per unit mass ϵ is given by

$$\epsilon = \alpha V_c^3 / r_c \tag{9.80}$$

where we take the maximum velocity and the core radius V_c and as the outer scale characteristic velocity and scale. Since a characteristic kinetic energy per unit mass is $V_c^2/2$, the turbulent decay time is proportional to

$$\tau_T \sim V_c^2/2G = \frac{1}{2\alpha} \frac{a}{V_c} \tag{9.81}$$

$$= \frac{a^2}{\alpha} \frac{\pi}{\Gamma_c}$$

Since the initial core radius α is proportional to the vortex separation b ($a \sim 0.098b$)

$$\tau_T \sim \frac{1}{4} \frac{2\pi b^2}{\Gamma_c} = \frac{1}{4} \frac{\Gamma}{\Gamma_c} \left(\frac{2\pi b^2}{\Gamma}\right) \tag{9.82}$$

where Γ_c is the core circulation. This time should be compared to the mutual instability growth time $\tau(b)$

$$\tau(b) = 2\pi b^2/\Gamma \quad . \tag{9.83}$$

Thus the characteristic turbulent diffusion time τ_T is directly proportional to the instability growth time:

$$\tau_T = \frac{1}{4} \frac{\Gamma}{\Gamma_c} \tau(b) = \text{constant x } \tau(b). \tag{9.84}$$

The presence of a ground plane does not alter the resulting conclusion that there is only one characteristic time in this cylindrical problem The effect of viscous interaction my be roughly evaluated as follows. We assume a vortex moving horizontally at a height b/2 above the ground. A turbulent bounday layer develops at a height b/2 above the ground. A turbulent bounday layer develops at the ground surface and grows upwards by turbulent diffusion. The characteristic time for friction with the ground to significantly alter the vortex motion is of the order of the time required for the bounday layer to grow to a thickness of order b/2. If the instantaneous boundary layer thickness is denoted by Δ , then the turbulent diffusivity ν_T is of order

$$\nu_T \approx \alpha V_g \Delta \tag{9.85}$$

where V_g is the velocity at the ground plane expected in the absence of the boundary layer ($V_g \sim 2\Gamma/\pi b$) and α is a small quantity which depends only weakly on Reynold's number (i.e. on time). To order of magnitude

$$\frac{d}{dt}(\Delta^2) \sim 4\nu_T \tag{9.86}$$

or

$$\frac{d\Delta}{dt} \sim 2\alpha(2\Gamma/\pi b) \tag{9.87}$$

and Δ will grow to the value b/2 in a time

$$\tau_g \sim \frac{2\pi b^2/\Gamma}{16\alpha} = \frac{\tau(b)}{16\alpha} . \tag{9.88}$$

Since α is essentially a constant parameter the turbulent ground interaction time can be taken to be (roughly) a constant factor times the instability time τ.

In the previous discussions we have treated the downstream variation of the trailing vortices from an aircraft flying at constant velocity as equivalent to the time dependent decay of a pair of cylindrical vortices. Thus no effect due to axial gradients has been considered. The inclusion of axial velocity and pressure gradients introduces a new characteristic time (i.e. a characteristic axial distance).

Dimensional analysis in the infinite Reynolds number limit ($\nu_{laminar} = 0$) shows that the circulation at t ($=Z/U_\infty$) after passage of the aircraft has a radial distribution of the form

$$\frac{\Gamma(r,t)}{\Gamma_\infty} = f\left(\frac{2\pi U_\infty^2 t}{\Gamma_\infty}, \frac{8\pi r^2}{\Gamma_\infty t}\right)$$
$$= f\left(\frac{2\pi U_\infty^2}{\Gamma_\infty} + \left(\frac{2r}{b}\right)^2 \frac{\tau}{t}\right) \qquad (9.89)$$

where we have chosen to write the second term so as to exhibit explicitly the expected dependence on the instability time $\tau = 2\pi b^2/\Gamma_\infty$. Thus we are led to consider the possibility that the wake is characterized by two times τ and τ_1 :

$$\tau = 2\pi b^2/\Gamma_\infty$$
and
$$\tau_1 = \Gamma_\infty/2\pi U_\infty^2 \qquad (9.90)$$

As will be shown the second term is probably associated with the phenomenon of "vortex breakdown". The ratio of these two times is a dimensionless number which characterizes the flow:

$$\beta = 4\pi^2 \tau_1/\tau = \left[\Gamma_\infty/U_\infty b\right]^2 \qquad (9.91)$$

and is related to the square of a swirl angle. Writing Γ_∞ as $2\pi a V_c$ where V_c measures the peak tangential velocity at the edge of the core we have

$$4\pi^2 \tau_1/\tau = \left(\frac{2\pi a}{b}\right)^2 \left(\frac{V_c}{U_\infty}\right) = 0.4 \ (V_c/U_\infty)^2. \qquad (9.92)$$

The time dependent cylindrical vortex model corresponds to the limit $V_c >> U_\infty$ or $\tau_1/\tau \to \infty$ and is applicable to very strong circulations. The opposite limit of $\tau_1/\tau \to 0$ occurs for small circulations in high speed flow.

There is experimental (and theoretical) evidence in laminar flows to indicate that a critical value of β obtains when V_c/U_∞ is of order unity. This is the threshold for vortex "bursting" or "breakdown". For aircraft vortices the value of V_c/U_∞ is usually small (~0.1) so that we might expect that the critical time τ_1 would be small compared to τ and that most of the flow could be described by the $\tau_1/\tau = 0$ limit. In this case we would expect diffusion effects to dominate and that the circulation would obey a simple similarity law of the form

$$\frac{\Gamma(r,t)}{\Gamma_\infty} \approx f\left(\left(\frac{2r}{b}\right)^2 \frac{\tau}{t}\right) \qquad (9.93)$$

However, this is actually not the case. The experiments and theory in which the critical ratio of $V_c/U_\infty = 1$ was found were experiments in which the axial velocity was more or less uniform in the radial direction. However, for aircraft vortices the low pressure in the core can give rise to strong axial

convection and it can be shown that near the wing the axial velocity in the core may be actually comparable to the peak tangential velocity. At the present time there is available little theoretical or laboratory experimental data on flows of this type. The data that is available indicates that vortex breakdown does occur in some aircraft wakes but there is some experimental evidence that the late time history of the vortex can be characterized by simple turbulent diffusion. Additional experiments and theory are required to establish models for the near wake and the aircraft parameters which establish the critical values of the time ratio τ_1/τ.

However, as far as induced rolling moments and aircraft hazard is concerned it is primarily the late time phenomena that is important. Here similarity solutions in the variable $(2r/b)^2(\tau/t)$ are valuable. These solutions should result by taking the limit of small perturbations to the axial flow ($\delta\omega/\omega << 1$ or $v/\omega << 1$ and $u/\omega << 1$) and are discussed in Section .

It is to be noted that, when considering simulation experiments, two requirements must be met. First, the laboratory dimensions must be large enough that the effects of molecular viscosity are negligible. This is equivalent to requiring conditions such that, in the turbulent portion of the flow, an appreciable inertial subrange exists. Second, the value of the swirl parameter $2\pi U_\infty b/\Gamma_\infty$ be kept in the same range as in the full scale phenomena. Experimental configurations that can accomplish these conditions are discussed in Section X.

X. WAKE MODELING AND SIMULATION.

In considering laboratory experimental simulations of the aircraft wake, the major considerations are to choose configurations that satisfy the condition of Reynolds number insensitivity and that allow the swirl parameter $2\pi U_\infty/\Gamma_\infty$ to be reproduced. We have considered three possible laboratory systems: an air tunnel, a water tunnel, a water tow tank or tow basin. In Table __ we list the values of various characteristic parameters for several different aircraft and in Table __ the comparable quantities for a selected set of laboratory configurations. The swirl parameter was chosen to reproduce a typical flight value and the water and wind tunnel flow rates were chosen so as to result in comparable power requirements and comparable test section lengths. All these experimental configurations appear possible to implement. However, the tow basin appears to be the simplest and the least expensive procedure, and the one that is most adaptable to studies of ground interaction, obstacles, and the effects of ambient turbulence.

The different experimental techniques are comparatively evaluated in this section.

Fig 10.1 Towing Basin for Wake Simulation

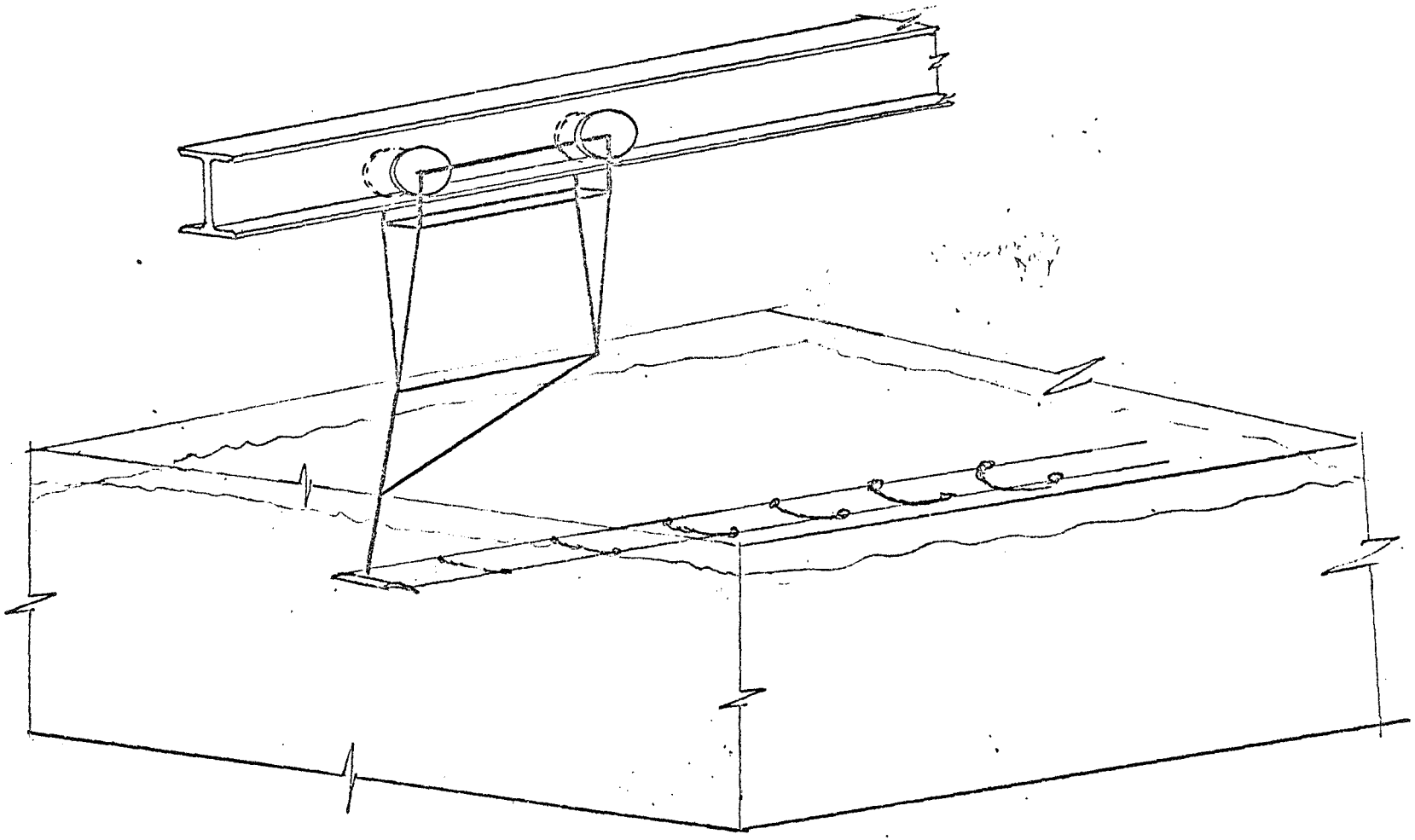

Fig. 10.2 Detail of towing basin simulation measurement.

Table 10.1: Wake Parameters for Various Aircraft (Take off conditions - maximum load) (based on the cylindrical vortex model)

Aircraft	737	727	707	747	C-47 (DC-3)
Weight (lbs)	104,000	161,000	336,000	710,000	29,300
Wing Span (ft)	93	108	146	196	95
Velocity (ft/sec)	260	255	284	294	~ 150
Vortex Circulation (for L=W: ft^2/sec)	2,360	3,220	4,480	6,800	800
Vortex Separation (ft) $\left(b = \frac{\pi}{4} \text{ (span)}\right)$	73.1	84.8	115	154	72
Initial Core Diameter (ft) (= 0.197 b)	14.3	16.6	22.7	30.4	14.4
Characteristic wake decay time (sec) $\left(\tau = 2\pi\rho Vb^3/W = 2\pi b^2/\Gamma\right)$	14.1	13.7	18.2	21.6	42
Centerline downwash velocity (ft/sec) (= $2\Gamma/\pi b$)	20.6	24.2	24.8	28.2	7.3
Peak vortex tangential velocity (ft/sec) (= $\Gamma/2\pi a$)	52.5	61.1	63.2	72.0	18

Table 10.1 Wake Parameters (continued)

Aircraft	737	727	707	747	C-47
Peak vortex tangential velocity (ft/sec) ($= \Gamma/2\pi a$)	52.5	61.1	63.2	72.0	18
Vortex translational velocity (ft/sec) ($= \Gamma/2\pi b$)	5.1	6.0	6.2	7.1	1.8
Core angular velocity (rps) $\frac{\Omega}{2\pi} = \frac{\Gamma}{(2\pi a)^2}$ $= 16.4/\tau$	1.16	1.17	0.89	0.75	0.40
Swirl parameter $(2\pi U_\infty b/\Gamma)^{-1}$	.0198	.0237	.0218	.0239	.011

Table 10.3: Configurations considered for experimental simulation

Flight	Circulation Γ	Vortex Separation (b)	Speed (V_o)	Kinematic Viscosity ν
(A):	9000 ft^2/sec	200 ft	300 ft/sec	0.15 cm^2/sec
(B):	3000	100	200	0.15

Laboratory				
Wind tunnel:	3000 cm^2/sec	10 cm	2000 cm/sec	0.15 cm^2/sec
Water tunnel:	300	10	200	0.01
Tow basin:	300	20	200	0.01

Table 10.4: Comparison of wake parameters

	Flight		Laboratory		
	A	B	Wind tunnel	Water tunnel	Tow basin
Velocity	300 ft/sec	200	2000 cm/sec	200	200
Circulation	9000 ft^2/sec	3000	3000 cm^2/sec	300	300
Vortex separation (b)	200 ft	100	10 cm	10	20
Characteristic wake Time	28 sec	20	0.2 sec	2	4
Experiment time	140 sec	100	1.0 sec	10	20
Characteristic wake length	8400 ft	4000	4.0 m	4	8
Experiment length	42000 ft	20000	20 m	20	40
Initial core diameter	40 ft	20	2 cm	2	4
Centerline downward velocity	60 ft/sec	20 ft/sec	200 cm/sec	20 cm/sec	10 cm/sec
Peak vortex tangential velocity					
Vortex translational velocity	15 ft/sec	5	50 cm/sec	5	5
Core angular velocity (rps)					

Table 10.4 (continued)

	Flight		Laboratory		
	A	B	Wind tunnel	Water tunnel	Tow basin
Swirl parameter	.023 ft/sec	.023	.023 cm/sec	.023	.023
Diffusion parameters Reynolds number	5×10^5	1.6×10^5	3000	5000	10000
$\left(\frac{\ell_{inner}}{a}\right)_{turbulent}$	$\frac{1}{7000}$	$\frac{1}{3500}$	$\frac{1}{140}$	$\frac{1}{230}$	$\frac{1}{460}$

Comparison of various experimental configurations

The principal advantage of a wind or water tunnel is that a steady state flow can be produced. Measurements can be carrie out at the leisure of the experimentalist and this generally permits detailed probing of the flow. However, since the tunnel walls do not move relative to the wing the viscous interactions with the ground plane cannot be properly simulated.

In a towing tank or basin where the wing is moved through a stationary fluid it is possible to obtain a direct simulation of the wake. Here the wing can be towed at a fixed angle of attack, fixed depth and fixed speed, and the wake can be observed at various fixed stations. Since the flow is unsteady after wing passes the observation time is limited and controlled by the experimental conditions. The wing moves past the fixed walls so that the ground interaction can be properly effected. Thus, although the unsteady characteristics of the towing basin limit the amount and detail of the data that can be obtained at a given time, it generally provides a better and more versatile simulation facility. Also when power requirements and fluid mass flow rates are limited, the tunnel operating costs can be significant, whereas the power requirements for a towing system are expected to be negligible. Estimates of the power required in order to combat frictional losses in wind or water tunnel boundary layers are given in the following section.

Wind/Water Tunnel Boundary Layers

The displacement thickness of the tunnel wall boundary layer at the end of the test section (length L) is given by

$$\delta_1 = 0.046\, L/(Re(L))^{1/5} \quad : \quad \text{Turbulent} \qquad (10.1)$$

$$\delta_1 = 1.721\, L/(Re(L))^{1/2} \quad : \quad \text{Laminar} \qquad (10.2)$$

Values of this thickness for the tunnels considered are given in Table 10.5.

Table 10.5: Boundary Layer Displacement Thickness

	ν	U_∞	L	Re(L)	δ_1 (turbulent)	δ_1 (laminar)
Air	0.15 cm^2/sec	20 m/sec	20 m	2.7×10^7	3.0 cm	0.66 cm
Water	0.01 cm^2/sec	2 m/sec	20 m	4.0×10^7	2.8 cm	0.54 cm

The transition from a laminar to a turbulent boundary layer occurs at a critical Reynolds number between 3×10^5 and 3×10^6 (depending on the level of free stream turbulence). For the tunnel flow conditions considered therefore the transition is expected somewhere between 0.3 and 3 meters from the entrance. For practical purposes we may thus take the boundary layer to be always turbulent.

For a 1m x 1m tunnel the test section area for both the air and the water tunnel is effectively reduced by the growth of the turbulent boundary by about 7% at the midpoint in the test section (10 meters) and by about 12% at the end of the section. The edge of the boundary layer extends into the flow a distance equal to 8 times the displacement thickness (i.e., 20 - 25 cm at the end of the test section). Since the lateral motion of the vortices for a 10 cm span wing is expected to be about 50 cm in the regime of prime experimental interest, a 1 m^2 test section appears to be reasonable for both the air tunnel and the water tunnel.

Power required for recirculating tunnels

The turbulent skin friction drag on the test section is given by

$$D = 0.036\ \rho U_\infty^2 A/[Re(L)]^{1/5} \tag{10.3}$$

where A is the wetted surface area and L the test section length. Thus the power required to drive the flow through the test is

$$P = 0.036\ \rho U_\infty^3 A/[Re(L)]^{1/5} \tag{10.4}$$

and for our nominal tunnels

$$\begin{aligned} P_{air} &= 3.0\ KW \\ P_{water} &= 2.8\ KW \end{aligned} \tag{10.5}$$

Depending on the design of the pumps and return sections of the tunnels the total pump power required is probably between 2 and 4 times the test section requirements (i.e. 6 to 12 KW) and is not unreasonable in terms of cost. An air tunnel does not need to be a closed system, although when smoke or tracers are to be injected an open system would have to be vented to the outside atmosphere and probably require an isolated facility.

For any sort of extended studies a water tunnel must, however, be recirculating since the water consumption otherwise is excessive (at a water cost of 50¢/1000 gallons, the operational volume flow rate of 2000 kg/sec (= 500 gallons/second) would yield a running cost of about $900/hour due to water value alone).

The power losses in the pump due to skin friction tend to vary as U_{max}^2 (i.e., as A_{min}^{-2}) where A_{min} is the minimum cross sectional area in the pump. Thus the diameter flow passages cannot be reduced much below 1 meter without incurring excessive power requirements. Mechanical pumps that can handle this high volume, low speed flow without requiring excessive power tend to be physically large and bulky.

The principal conclusions that can be drawn are the following. Both air and water tunnels appear to have comparable capability for simulating the trailing vortex wake. The power requirements are comparable and are moderate. The facilities required in both cases are moderately large particularly because of the requirements for test section length (a 60 foot long test section with a return system probably requires a floor area at least 30 by 80 feet). Test sections of the required length are not normally available in the existent facilities and a moderate amount of construction would be involved to modify a presently operational tunnel. Thus, although it appears that there are no major technical problems involved in constructing or modifying an air or water tunnel facility and that the performance that could be achieved would provide an adequate simulation of the full scale phenomena, the required amount of new construction is considerable.

The alternate approach of a water tow tank offers a number of advantages. Here a 2m x 4m channel is envisaged that is 100 meters long. A wing mounted on a carriage running on rails extending the length of the channel is towed at constant velocity down the channel.

The wake is observed as an unsteady phenomenon from various fixed stations along the two basin. A number of appropriate facilities exist in the country and can be used essentially without modification. Required construction includes the wing assembly and its support, the dye injection apparatus and the appropriate assembly to mount the apparatus on the tow basin carriage. Since the dimensions of the tow basin are not critical cost factors it is possible to use larger models and achieve higher Reynolds numbers than are possible in tunnels.

The major disadvantage of the tow basin is that the flow is unsteady and the time available for measurements is limited. Thus for detailed probing of the wake a tunnel is probably preferred. However, for preliminary measurements aimed at establishing the validity of various phenomenology models and for establishing the validity of the simulation, the tow basin appears to be an effective approach.